Université de Montréal

Poly(ethylene-co-acrylic acid) random copolymers: amphiphilic properties and self-assembly in aqueous medium.

par
Volodymyr Kriuchkov

Département de Chimie
Faculté des arts et des sciences

Mémoire présenté à la Faculté des arts et des sciences
en vue de l'obtention du grade de Maîtrise en sciences
En chimie

Janvier 2011

Université de Montréal
Faculté des études supérieures et postdoctorales

Ce mémoire intitulé:

Poly(ethylene-co-acrylic acid) random copolymers: amphiphilic properties and self-assembly in aqueous medium.

Présenté par:
Volodymyr Kriuchkov

a été évalué par un jury composé des personnes suivantes:

Antonella Badia, président-rapporteur
Françoise M. Winnik, directrice de recherche
William Skene, membre du jury

Résumé

Les travaux de recherche présentés ici avaient pour objectif principal la synthèse de copolymères statistiques à base d'éthylène et d'acide acrylique (AA). Pour cela, la déprotection des groupements esters d'un copolymère statistique précurseur, le poly(éthylène-co-(tert-butyl)acrylate), a été effectuée par hydrolyse à l'aide d'iodure de triméthylsilyle.

La synthèse de ce précurseur est réalisée par polymérisation catalytique en présence d'un système à base de Palladium (Pd).

Le deuxième objectif a été d'étudier et de caractériser des polymères synthétisés à l'état solide et en suspension colloïdale. Plusieurs copolymères précurseurs comprenant différents pourcentages molaires en tert-butyl acrylate (4 à 12% molaires) ont été synthétisés avec succès, puis déprotégés par hydrolyse pour obtenir des poly(éthylène-co-acide acrylique) (pE-co-AA) avec différentes compositions. Seuls les copolymères comprenant 10% molaire ou plus de AA sont solubles dans le Tétrahydrofurane (THF) et uniquement dans ce solvant. De telles solutions peuvent être dialysées dans l'eau, ce qui conduit à un échange lent entre cette dernière et le THF, et l'autoassemblage du copolymère dans l'eau peut ensuite être étudié. C'est ainsi qu'ont pu être observées des nanoparticules stables dans le temps dont le comportement est sensible au pH et à la température.

Les polymères synthétisés ont été caractérisés par Résonance Magnétique Nucléaire (RMN) ainsi que par spectroscopie Infra-Rouge (IR), avant et après déprotection. Les pourcentages molaires d'AA ont été déterminés par combinaison des résultats de RMN et

de titrages conductimètriques. A l'état solide, les échantillons ont été analysés par Calorimétrie différentielle à balayage (DSC) et par Diffraction des rayons X.

Les solutions colloïdales des polymères pE-co-AA ont été caractérisées par Diffusion dynamique de la lumière et par la DSC-haute sensibilité. De la microscopie électronique à transmission (TEM) a permis de visualiser la forme et la taille des nanoparticules.

Mots-clés: nanoparticules, Pd-catalyseurs, polyéthylènes, acide acrylique, DLS, HS-DSC

Abstract

The first objective of this research is to synthesize random linear copolymers of ethylene and acrylic acid (AA). The synthesis relies on the deprotection of the functional groups in the copolymer's precursor, which is represented by poly(ethylene-co-tertbutyl acrylate). The synthesis of the precursor was realized by the catalytic approach, where Pd-based catalytic systems are frequently utilized nowadays. The deprotection was carried out by hydrolysis of the ester functionality using trimethylsilyl iodide agent.

The second objective is to investigate and characterize the synthesized polymers in the bulk and in colloidal solution. A set of different precursor polymers with various degrees of molar incorporation of tertbutyl acrylate (from 4 to 12 mol %) was successfully synthesized and deprotected. The resulting poly(ethylene-co-acrylic acid) copolymers were found to be soluble in tetrahydrofuran THF, when the molar incorporation of AA reaches the value of 12 and more. This aspect gave the possibility to study the self-assembly of this copolymer in aqueous medium by slow THF to water exchange (dialysis). It was found that the copolymers self-assemble into nano-sized structures and these nanoparticles remain stable in colloidal solution for extended periods of time. Moreover, it was shown that the nanoparticles formed by the discussed copolymer possess thermo- and pH-responsive behaviour.

The polymers synthesized were characterized by nuclear magnetic resonance (NMR) and infrared spectroscopies (IR) before and after deprotection. The bulk samples were analyzed by conventional differential scanning calorimetry and by X-ray diffraction

technique. The molar percentages of AA were determined using a combination of NMR and conductimetric titration. Colloidal solutions of pE-co-AA copolymers were analyzed by dynamic light scattering and high-sensitivity differential scanning calorimetry techniques. The nanoparticles formed were visualized and characterized by transmission electron microscopy.

Keywords: nanoparticles, Pd-catalysts, polyethylenes, acrylic acid, DLS, HS-DSC.

Table of Contents

List of Abbreviations

AA	Acrylic Acid
ADMET	Acyclic Diene Metathesis Polymerization
$AlEt_3$	Triethylaluminium
Cp	Cyclopentadienyl
DSC	Differential Scanning Calorimetry
dn/dc	Differential Refractive Index Increment
ETM	Early Transition Metal
FTIR	Fourier-Transform Infrared Spectroscopy
FDASG	Finely Divided Aluminum Silicate Gel
GADDS	General Area Detector Diffraction System
HS-DSC	High-Sensitivity DSC
LTM	Late Transition Metal
MA	Methyl Acrylate ester
MAO	Methylalumoxane
NHC	Nucleophilic Heterocyclic Carbene
NMR	Nuclear Magnetic Resonance
pE	Polyethylene homopolymer
pE-co-M	Copolymer of Ethylene with M
PDI	Polydispersity Index
PENVP	Poly(ethylene-co-N-vinylpyrrolidinone)
RI	Refractive Index
ROMP	Ring Opening Metathesis Polymerization

TBA	Tertiary Butyl Acrylate ester
TEM	Transmission Electron Microscopy
TGA	Thermogravimetric Analysis
$TiCl_4$	Titanium (IV) Tetrachloride
THF	Tetrahydrofuran
TMEDA	Tetramethylethyldiamine
TMSI	Trimethylsilyl iodide

List of Tables

List of Figures

of PEMA (poly(ethylene-co-methyl acrylate) and PENVP, poly(ethylene-co-N-vinylpyrrolidinone), are taken from reference 32. The lines are to guide the eye.

Figure 2.3. TEM micrographs of nanoparticles obtained from dialyzed suspensions of PEAA12 (upper right: enlarged view of one of the particles; lower right: electron diffraction pattern obtained for one nanoparticle)

Figure 2.4. Thermograms of an aqueous dispersion of PEAA12 in water (~1 g/L) recorded by HS-DSC upon heating and subsequent cooling (heating/cooling rate: 1 ^{o}C/min). The arrows indicate the melting points of solid PETBA12 and PEAA12.

Figure 2.5. Hydrodynamic radii distributions recorded by DLS for a suspension of PEAA12 in water heated to various temperatures from 20 ^{o}C to 65 ^{o}C. The top trace corresponds to a sample cooled from 65 ^{o}C to 25 ^{o}C.

Figure 2.7-S1a. ^{1}H NMR of poly(ethylene-co-TBA) with 7 mol% of TBA. ($C_2D_2Cl_4$, T = 120 ^{o}C).

Figure 2.7-S1b. ^{1}H NMR of poly(ethylene-co-TBA) with 10 mol% of TBA. ($C_2D_2Cl_4$, T = 120 ^{o}C).

Figure 2.7-S1c. ^{1}H NMR of poly(ethylene-co-TBA) with 12 mol% of TBA. (C2D2Cl4, T = 120 ^{o}C).

Figure 2.7-S2. ^{1}H NMR of poly(ethylene-co-TBA) with 10 mol% of TBA. ($C_2D_2Cl_4$, T = 120 ^{o}C). Insert : vinylic end-groups. The resonance labeled e corresponds to internal double bonds generated upon isomerization of terminal double bonds. Such isomerization is well established for palladium aryl sulfonate catalysts: see for example comment about octene insertion.

Figure 2.7-S3. ^{13}C NMR (quantitative) of poly(ethylene-co-TBA) with 12 mol% of TBA. ($C_2D_2Cl_4$, T = 120 ^oC). Using the data of on the insertion polymerization of methyl acrylate and ethylene[3], three types of resonances are possible for **C**H($CO_2{}^tBu$): one for consecutive acrylate dyads AA at 42 ppm, one for alternated acrylate triads AEA at 44 ppm, and one for isolated acrylate units at 46 ppm. The *a* resonance is therefore indicative of isolated acrylate units, in agreement with a copolymer with a random distribution.

Figure 2.7-S4. GPC trace of poly(ethylene-co-TBA) with 7 mol% of TBA. (ODCB, T = 160 ^oC). Flow rate: 1 ml/min. Columns (2): Mixed C-LS Polymer Laboratories. Detectors: RI, viscometer and light scattering. Calibration: triple detection.

Figure 2.7-S5. ^1H NMR of poly(ethylene-co-AA) with 12 mol% of acrylic acid incorporation (THF-d^8).

Figure 2.7-S6. ^{13}C NMR of poly(ethylene-co-AA) with 12 mol% incorporation of acrylic acid (THF-d^8).

Figure 2.7-S7. FTIR of the polymers before and after treatment with TFA (C=O stretching region).

Figure 2.7-S8. FTIR spectrum of polymers before (top) and after ester hydrolysis (bottom, using TMSI activation).

Figure 2.7-S9. Changes in conductivity (**A**) and pH (**B**) as a function of added volume of HCl (0.02 M) for a solution of polymer with 17 mol% of acrylic acid, in THF/aqueous solution containing 0.02 M NaOH illustrating the determination of the carboxylic acid content in the polymer sample (see details in experimental section).

Figure 2.7-S10. Powder X-Ray diffractogram of poly(ethylene-co-AA) containing 7 mol% AA.

Figure 2.7-S11. Distribution of diameters for PEAA (x = 12%) nanoparticles analyzed by TEM (top : equatorial diameter, bottom : polar diameter).

Figure 2.7-S12 Representative Energy dispersive X-Ray spectrum of one of the nanoparticles of *Figure 2.3* (TEM above). The presence of Na is indicative of surface COONa groups. Cu, S, Si and Ca elements are present in virgin grids and are due to the carbon-formvar coating on the Cu grid.

List of Schemes

« If you make a mistake and do not correct it, this is called a mistake. »

Confucius

Acknowledgment

I would like to say here, that everyone who has supported me and helped me even in some small ways during my years at the University of Montreal must be acknowledged and I express my thanks to all of them personally.

Introduction

Motivation. The copolymerization of ethylene and polar monomers catalyzed by well-defined Late Transition Metal (LTM)-based systems presents an attractive synthetic approach for random linear copolymers. However, the incorporation of polar comonomers into the polyethylene backbone by this way establishes a substantial synthetic challenge, because the polar functional groups are favored to interfere with LTM catalytic center and decrease or completely cancel its activity. In spite of this fact, during the last decades significant progress has been done on design of the catalytic core and its ligand surrounding. Several synthetic approaches on linear ethylene copolymers bearing a variety of polar functional groups have been reported to date. This group of copolymers classified as amphiphiles, because their combine hydrophobic (polyethylene) and hydrophilic (polar groups) parts in one chain. Thus, amphiphilic polymers can self-assemble into a variety of nano-sized structures depending on the solvent environment.

Aims and Objectives. The aim of this research is to develop an amphiphilic copolymer based aqueous colloidal system with thermal and pH responsive behaviour. To this end the objectives of this thesis are:

1) Synthesize and characterize the linear random ethylene acrylate copolymers;
2) Study the bulk properties of copolymers synthesized;
3) Gain and establish their self-assebly in aqueous medium;
4) Study the properties of colloidal nano-structures formed.

Thesis Overview

Chapter one presents an introductory word into the world of functional polyethylenes, beginning from the very first report on polymethylene synthesis and finishing with the complex catalytic approach in synthesis of functional linear polyethylene copolymers. General methods used for characterization of this type of copolymers are presented here as well.

In Chapter two, the study of properties of pE-co-AA copolymers is presented as a full paper article, published in Journal of American Chemical Society on the basis of the work done by me during my studies.

Finally, Chapter three presents general conclusions, which summarize the research completed and suggest for further studies.

CHAPTER I

Introduction to polyethylenes and their characterization

1.1 Polyethylenes

1.1.1 Homopolymerization of ethylene

Origin. Polyethylene (PE) occupies a leading position among plastics in the world, with a total production of approximately 70 million tons per year or nearly half of all synthetic polymers. There exist several different types of PE classified by the amount of branching. Branching affects the physical properties of the polymer, in particular the density, the melting point, and the degree of crystallinity.

The history of PE takes us to the XIX century, when the first PE synthesis was carried out starting from diazomethane. The substance obtained was believed to be a poly(methylene) derivative[1,2]. After several reports on the spontaneous synthesis of high molecular weight hydrocarbons and what was called "polymethylene"[3-5], in 1934, PE was synthesized unexpectedly in an industrial environment upon application of high pressure to a mixture of ethylene and benzaldehyde[6]. This "spontaneous preparation" was later modified by Michael Perrin (Imperial Chemical Industries, Great Britain), who converted an uncontrolled procedure into a reproducible method. In 1937[7], ICI deposited the first patent for PE synthesis. The industrial production was started in 1939. Since then and until now, the PE significance in the world industry cannot be overlooked. PE played a key role in the development of packaging materials, dielectrics and is present in all aspects of everyday life.

Development. Much effort was spent on the development of the catalytic polymerization of ethylene (E). The first successful report was published in 1958 by Hogan and Banks (Philips catalyst, patented in the same year)[8]. Their work dealt with

chromium trioxide-based catalytic systems[9-12] and they were able to polymerize ethylene under milder conditions than free radical polymerization. The polymers obtained had narrow molecular weight distributions and a low degree of branching. Almost simultaneously, a catalytic system based on a mixture of titanium halides and organoaluminium compounds ($TiCl_4$ + $AlEt_3$) was developed for ethylene polymerization by the German chemist *Karl Ziegler* in 1953[13,14]. Subsequently, *Giulio Natta* in Italy reported the synthesis of isotactic polypropylene via *α-olefin catalytic polymerization* in 1955[15,16] using the same type of catalyst. The novel catalytic system could be used under milder conditions than the Phillips catalyst.

The Phillips catalyst system contains a chromium derivative, supported on a finely divided aluminum silicate gel (FDASG). After modification with a fluoride, it is activated in an oxidizing atmosphere at elevated temperatures. The FDASG (carrier gel) has an alumina content of 0.5 to 6% by weight, with alumina being concentrated on the surface of the carrier gel particles. With the Phillips' catalytic system, it is possible to synthesize more than 50 different types of high density and linear low density polyethylenes. In addition, the production process and catalyst preparation are simplified by the fact that these systems do not require activators.[17] The Ziegler-Natta catalyst normally contains a support (often based on anhydrous $MgCl_2$), a metal source ($TiCl_4$, etc.), one or two Lewis bases called *internal* and *external* Lewis bases (phthalates, siloxanes for example), and an alkyl aluminum.[18]

The invention of metallocene catalysis of ethylene polymerization led to a new era. Metallocenes like ferrocene, from which their name derive[19], contain a transition metal and coordinated in a *sandwich structure* two cyclopentadienyl ligands (Cp), i. e., they are

co-planar with equal bond lengths and strengths. The ability to polymerize ethylene with high activity was discovered in 1980[20] for metallocenes such as $ZrCp_2Cl_2$. The system was activated by methylalumoxane (MAO). It allowed the polymerization of ethylene as well as the preparation of high molecular weight copolymers of ethylene with other α-olefins[21,22].

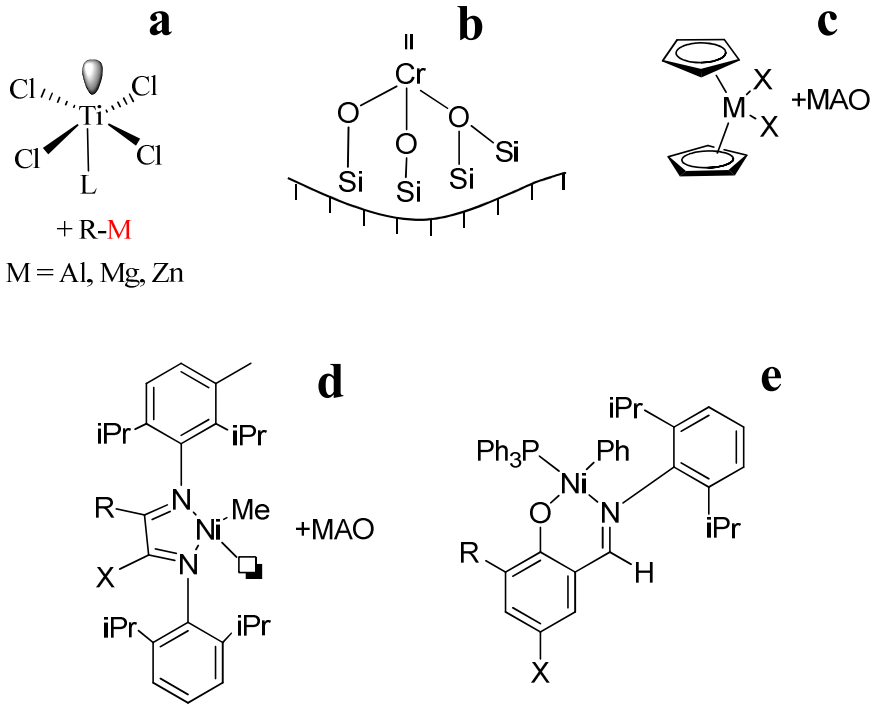

Figure 1.1.1. Structures of catalysts for ethylene polymerization: **a** – Ziegler-Natta type; **b** – Phillips type; **c** – Metallocene type; **d** – Brookhart complex; **e** – Grubbs complex.

1.1.2 Copolymerization of ethylene and polar monomers: branched derivatives

Impact. The main drawback of Ziegler-Natta and metallocene catalysts is related to the oxophilic nature of the early transition metals (ETMs) that constitute the catalytic complexes. The late transition metal (LTM) based catalysts are also known to polymerize ethylene in a controlled fashion. LTM based catalysts received much less attention than ETM due to the low catalytic activity of the olefin insertion and because they undergo rapid competitive β-hydride elimination from the alkyl-metal intermediate which results in formation of dimers or oligomers. In the mid-1990, *Maurice Brookhart* and colleagues

reported novel α-diimine Pd (II)- and Ni(II)-based complexes[23-25], which were able to catalyze the copolymerization of ethylene and alkylacrylates and to generate hyperbranched copolymers with acrylate functions located preferentially at the branching ends as a consequence of *chain-walking mechanism*. This invention demonstrated that the insertion of polar functionalities into late transition metal alkyl species has a dramatic effect on the polymerization process. The other key features of this polymerization system are that the character and content of branching depend on the reaction conditions.[26-37]

Development. The Brookhart type catalysts include neutral Ni/Pd complexes with aryl N,N-diimine ligands bearing bulky substituents in the *ortho* positions of the aryl rings (*Figure 1.1.1d*), activated with co-catalysts or activators, i.e. diethyl aluminum chloride (DEAC), MAO. These ligands play an important role in the stabilization of organometallic complexes that can be prepared by simple condensation reaction between alkyl/arylamine and diketone.

These catalysts are highly efficient in the homopolymerization of ethylene yielding branched (Ni) and hyperbranched (Pd) polyethylenes. However, the Lewis acid activity and interaction of alkyl aluminum co-catalysts and activators with polar monomers such as acrylates make them unsuitable for the copolymerization of ethylene with acrylates. To overcome this shortcoming, *Brookhart et al.* developed well-defined cationic species, in which the counterion was a fluorinated arylborate like *trityl tetrakis-(pentafluorophenyl) borate*. At comparatively low methyl acrylate feed, the nickel catalysts gave linear copolymers, where acrylate incorporation was very low.

Later, MacLain *et al.* (a group from DuPont) reported that it was possible to prepare linear copolymers of ethylene and acrylates with the Brookhart catalysts by increasing the ethylene pressure to 1000 psi, followed by the addition to nickel of a large excess (×200-300) of the expensive Lewis acid, *tris-(pentafluorophenyl)borane*.[38] However, the yields were poor, the acrylate incorporation was less than 6 mol% and the molecular weights were low (<8000 g/mol). The required high pressure and enormous cost of the Lewis acid utilized to diminish the *polymer back-biting* problem represented considerable obstacles on the way to commercialization.

Pd-based catalytic systems were the first systems able to copolymerize directly ethylene and acrylates. A schematic reaction of methyl acrylate (MA) insertion into these catalysts is shown on *Scheme 1.1.1*. The first step involves the coordination of the olefinic moiety of MA onto the cationic metal (Pd).

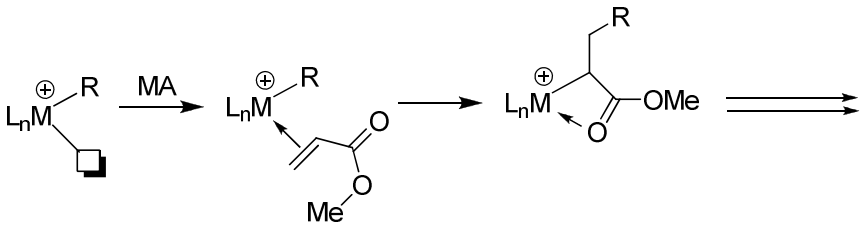

Scheme 1.1.1. The process of acrylate insertion into the Brookhart-type catalyst[39].

Then, migration insertion of the MA monomer into the Pd-carbon bond occurs in a 2,1-insertion way to form the resulting insertion product. The geometry and the electrophilicity of the metal center lead to a stiff coordination of the carbonyl functionality of the inserted acrylate comonomer. This “rapid blocking” prevents further polymerization, since, by occupying the vacant site critical for coordination, subsequent insertion of the next monomer unit is prevented. It was found that “chain-walking” of the Pd center resulted in the migration of the catalyst away from the polar group with further

ring expansion and precipitation of the complex from the reaction mixture. The chain-walking that follows every acrylate insertion results in hyperbranched polyethylenes with acrylate end groups rather than the desired linear PE with random incorporation of acrylate functionality.

The Pd-catalytic materials might be useful in a number of specialty applications such as those explored by *Guan et al.*[40-42] who used cyclophane-based Pd(II) α-diimine catalysts. The research group synthesized different types of materials with dendritic morphology, which could find possible applications as processing aids, rheological modifiers and amphiphilic core-shell nanoparticles as drug delivery systems.

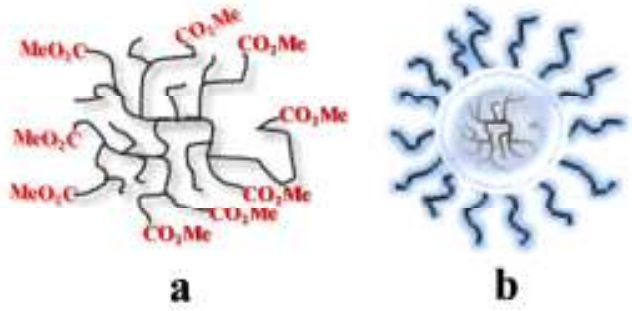

Figure 1.1.2. Dendritic copolymers prepared via chain-walking mechanism: **a** – branched PE with acrylate functionalities as a branch termination point; **b** – amphiphilic core-shell structure of the polymer as a result of self-assembly in aqueous environment (pE core and polar corona).

Later, the group of Guan optimized these catalysts by introducing very bulky cyclophane diimine palladium (II) complexes[29,42] that showed greater activity and stability than their acyclic analogs. The incorporation levels of acrylates (*tert*-butyl and methyl acrylate) were higher (up to around 25 mol%), compared to copolymers obtained by acyclic catalyst. The insertion energies of ethylene and MA are very close for both

catalytic systems. This fact was proved by low-temperature NMR spectroscopy. The authors conclude that the substitution of ligand is considerably hindered by the bulky cyclophane and the reduction in monomer exchange speed, relative to the monomer insertion, largely deduces the ability of the catalyst to discriminate between comonomers, resulting in high levels of acrylate incorporation in the final ethylene copolymers.

1.1.3 Copolymerization of ethylene and polar monomers: towards linear derivatives

Reducing the electrophilicity of the metal center may improve the properties of the catalyst. *Ziegler*[31] reported that the interaction of acrylate ester group with the metal center is weaker in neutral complexes, compared to the corresponding cationic complexes. Meanwhile, a neutral Ni-based system was reported by *Grubbs et al*.[43] The catalyst is tolerant to polar groups and capable to copolymerize ethylene with monomers such as norbonenes with ester functionality. The system is ineffective for acrylates, apparently because coordination of the ester group is stronger with Ni (II) than with Pd (II). Besides the use of neutral metal complexes it is also necessary to isolate the catalytic center by using bulky ligands. Making the catalytic center dense enough has two benefits. First, the binding of the last inserted ester functionality will be diminished or prevented. Second, it might be possible to override the electronically preferred 2,1-insertion of acrylates to the less sterically demanding 1,2-insertion. The growing polymer chain does not have ester functionality at the α-carbon, making it more nucleophilic and relieving the next insertion step.

Modeling calculations of the energy barriers for 1,2- and 2,1-insertion of methyl acrylate into Brookhart-type diimine complexes carried out by *Ziegler*[44] show that for

sterically unhindered catalysts 2,1-insertion has a significantly lower energy (by 4.5 kcal mol^{-1}) than 1,2-transition state. However, for a typical hindered catalyst, 2,1-insertion is only marginally favored (by 0.5 kcal mol^{-1}) over 1,2-insertion.

In several studies, *Grubbs et al.*[28,34-36,45] replaced the phenoxyimine ligands (used in their initial study) with nucleophilic heterocyclic carbene (NHC) ligands, aiming to push more electrons into the metal center, to reduce the tendency of the last-inserted acrylate monomer to coordinate the catalyst and retard further reaction (*Scheme 1.1.1*). These chelating NHC ligands are very hard to synthesize, as was the synthesis of the metal complexes, because the carbenes usually decomposed through the ring-expansion pathway[35]. As soon as the targeted NHC metal complexes were obtained and tested, they were found to be inactive in polymerization of olefins, showing that the electron-donor power of the NHC ligand makes the coordination of ethylene by the metal center more favorable. The first examples of a transition metal-catalyzed incorporation of acrylate monomers into linear polyethylene were demonstrated in 2002, by *Drent and colleagues*[27] who described the use of neutral Pd catalyst with chelating P-O ligands to generate linear copolymers of ethylene and acrylate monomers (*Scheme 1.1.2*). In these preliminary results, there was only low acrylate incorporation (limited to some 3-17 mol%) and the resulting copolymers were of quite low molecular weight (4000-15000 Da).

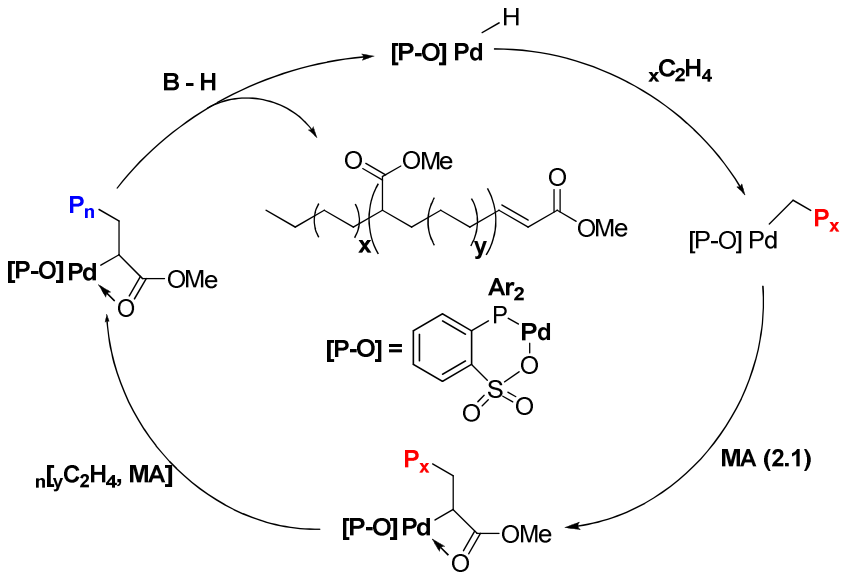

Scheme 1.1.2. Drent's catalyst and the proposed catalytic cycle for ethylene/methyl acrylate copolymerization[27,39].

The catalyst was generated *in situ* by mixing with the ligand, a Pd source which is broadly defined as a complex of Pd (0) or any other form of Pd metal forming an active catalyst upon mixing. In particular, Drent used *tris-(dibenzylideneacetone) dipalladium(0) ($Pd_2(dba)_3$), bis(dibenzylideneacetone) palladium(0), or palladium(II) acetate.*

$Pd(dba)_2$ [palladium(0)] generally gives the best results. The mechanism is believed to involve oxidative addition of the acidic phosphonium P-H moiety (*Scheme 1.1.3.1*).

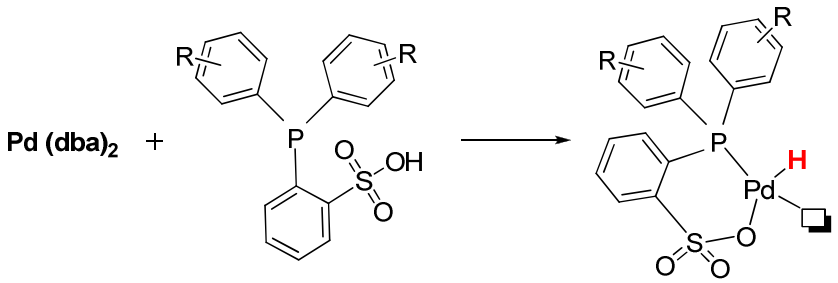

Scheme 1.1.3.1. Proposed mechanism for the formation of Pd (0) compounds[39,46].

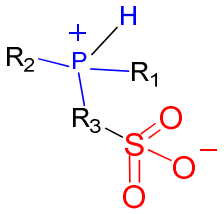

Scheme 1.1.3.2. Zwitterionic nature of the sulfonic phosphine ligand[39,46].

Reactivity patterns of this *in situ* method are in agreement with the hypothesis that Pd oxidation occurs via the acidic phosphonium. This initial reaction would involve the formation of Pd hydride. Such hydride intermediates are very reactive. As noted above, the ligand contains an acidic phosphonium hydrogen and can further react with the initially formed Pd-H species to form a "bischelated complex" (two ligands per metal) as shown in *Scheme 1.1.4*. This bischelated Pd is dormant during further polymerization.

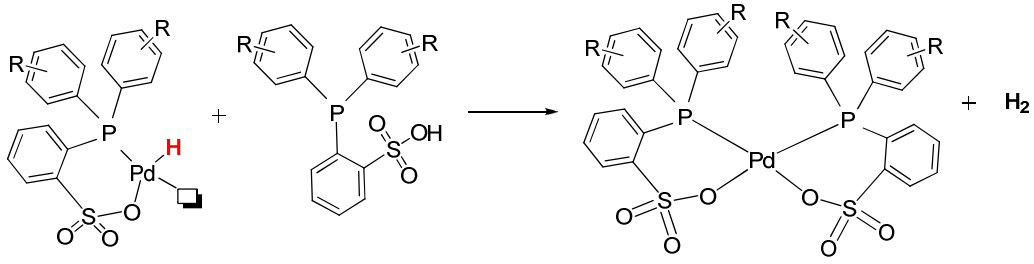

Scheme 1.1.4. Proposed reaction of Pd-H moiety reacting with excess ligand to form the inactive bis-chelated complex[39].

Indeed, the formation of bischelated products is a common problem of the general class of neutral, square-planar, late transition metal catalysts ("Keim-type" catalysts[47]). *Grubbs et al.*[36] have provided an example of bischelated nickel catalysts which were designated for the same aim of ethylene copolymerization with polar monomers *(Figure 1.1.3)*.

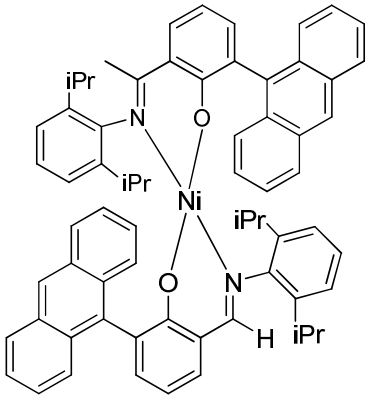

Figure 1.1.3. Bis-chelated Ni complex[39].

The problems associated with the *in situ* approaches can be avoided by using a preformed catalyst. The monometallic Pd catalyst is constituted with sulfonated phosphine ligand chelated to a Pd from one side and a Pd-carbon bond from another side (alkyl/aryl radical – growing polymer chain), most probably in the *cis* position with respect to the phosphorous (*Figure 1.1.4*).

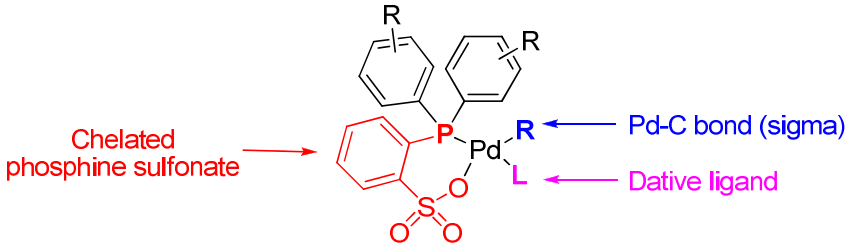

Figure 1.1.4. Key features of well-defined neutral palladium complex[39,46].

Thus, the requirements for a well-defined discrete complex are:

1) Be stable and recoverable;

2) Contain a Pd-carbon σ-bond (alkyl or aryl);

3) The ligand is chelated to the metal center;

4) Contain a weak donor auxiliary ligand that is readily replaced by incoming olefinic monomers (*Figure 1.1.4*).

As soon as prepared, the ligands alone contain an acidic phosphonium moiety with a *pKa* approximately 3 (*Scheme 3.2*). Employing this acidic group to withdraw a proton from an alkyl or aryl group from Pd represents a clean synthetic method[48] with tetramethylethyldiamine Pd (II) dimethyl, (TMEDA $PdMe_2$), as a convenient and storage-stable Pd precursor. The resulting catalytic complex is a stable crystalline solid in the form of the pyridine adduct (L, the auxiliary dative ligand in *Figure 1.1.4* is pyridine) by adding a stoichiometric amount of pyridine to the mixture prior to drying and isolating the product.

The resultant complexes can be efficiently used as single component catalysts in the homopolymerization of ethylene or its copolymerization with acrylates[48] and a variety of other polar monomers, such as vinyl ethers, vinyl fluoride[30], N-vinyl-2-pyrrolidinone, and N-isopropylacrylamide[49-51]. In fact, the above mentioned catalysts are so strong that they can be utilized as single component catalysts in the copolymerization of ethylene with norbonenes and acrylates[50,51] carried out in aqueous emulsion.

1.1.4 Functionalized polyethylenes: other synthetic approaches

Chemical modification of pre-formed polyethylenes by postpolymerization functionalization is frequently used to prepare various linear PEs. Generally, the method demands harsh reaction conditions because of the inert nature of polymer C–H bonds[52].

Recently, the ring-opening metathesis polymerization (ROMP) of functionalized cyclooctenes was shown to be effective in producing functional, linear polymers[53,54]. Because of the formation of polyunsaturated linear polyethylenes, a subsequent hydrogenation is required to make them saturated. Acyclic diene metathesis polymerization (ADMET) of symmetrically substituted α,ω-dienes followed by hydrogenation were also developed for preparing functionalized linear polyethylenes[55,56]. In both cases, the polymers have a linear backbone. The incorporation of polar monomers varies from random to sequential. The main disadvantages of this approach are the requirements of specifically prepared monomers and their multiple step preparation.

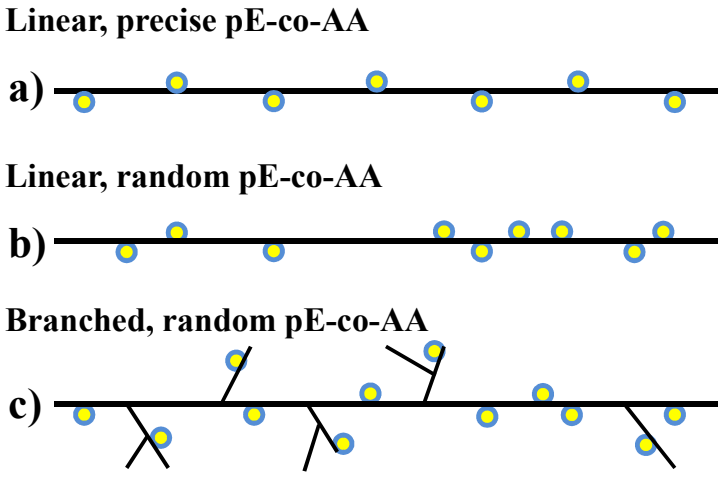

Figure 1.1.5 Linear poly(ethylene-*co*-acrylic acid) copolymers with (a) acid groups separated by a precisely controlled number of carbon atoms synthesized via ADMET and (b) acid groups with pseudorandom spacings synthesized via ROMP. (c) Branched

poly(ethylene-*ran*-methacrylic acid) copolymers with randomly spaced acid groups commercially produced using high-pressure polymerization (figure is inspired by Reference 57).

1.1.5 Ethylene copolymers as amphiphiles

Amphiphilic copolymers are macromolecules with both hydrophilic and hydrophobic parts. These parts may be randomly distributed along the linear/branched main chain or organized into blocks. Due to two different functionalities combined in the same chain, the behaviour of the polymer depends on its environment. Such behaviour is based on the microphase separation of the chemically different units which constitute the macromolecule.

Functionalized polyethylenes possess amphiphilic character due to hydrophobic properties of pE and hydrophilicity of functional group segments. In the aqueous medium, amphiphilic PEs are able to self-assemble into a variety of nanostructures such as unimolecular micelles, vesicles, etc[57,58]. The morphology of the structure formed depends on the ratio between hydrophobic/hydrophilic substitution incorporations, the nature of the functional group and the molecular weight of the copolymer. In addition, the tendency of pE to crystallize represents another driving force in the self-assembly of functionalized polyethylenes in aqueous medium.

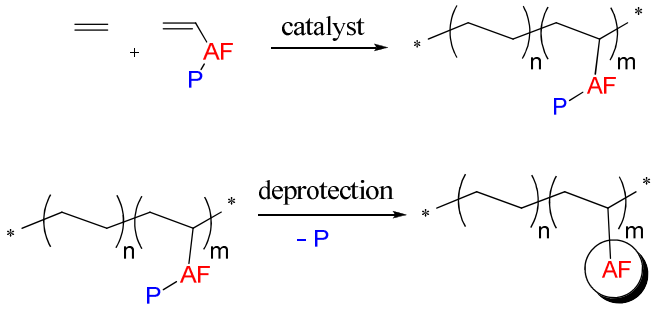

AF - Active Functionality

P - Protection group

Scheme 1.1.5. An example of synthesis of functionalized polyethylene via catalytic copolymerization of ethylene and functional α-olefin.

1.2 General Methods of Characterization of PE copolymers

1.2.1 Thermal Gravimetric Analysis and Differential Scanning Calorimetry [59-62]

Thermal analysis techniques monitor the physical properties of a substance as a function of temperature.

In *Thermal Gravimetric Analysis* (TGA), the mass of a sample under controlled atmosphere is recorded continuously as a function of temperature or time as the temperature of the sample is increased. A plot of the mass or mass percentage as a function of time or temperature is called a thermogram or a thermal decomposition curve. Commercially available Thermal Gravimetric Analysis instruments consist of four main components. The first one is a *high precision microbalance (thermobalance)* with a pan (generally platinum), where the sample is loaded for analysis. A number of different thermobalance designs available commercially are capable of providing quantitative information about samples ranging in mass from less than 1 milligram to 100 grams. Typically the range is 1 to 100 mg. Many thermobalance models can detect changes in mass as small as 0.1 microgram. The sample holder is housed in a furnace; the rest of the balance must be thermally isolated.

The second component is *the furnace,* consisting of a small electrically heated oven with a thermocouple to measure the temperature accurately. TGA furnaces typically cover the range from ambient temperature to 1000 ºC, but temperatures up to 1600 ^{o}C can be used in some cases. Heating or cooling rates can be selected from 0.1 ºC/min to 100 ºC/min. Some units can use rapid heating rate such as 200 ºC/min. Insulation and cooling

of the exterior of the furnace is required to avoid heat transfer to the balance. Nitrogen or another inert gas is usually used to purge the furnace and prevent oxidation of the sample. In some analyses it is possible to switch purge gases as the analysis proceeds. After analysis, furnaces are usually cooled by pressurized air and the cooling period from 1000 ^{o}C to 30 ^{o}C may last less than 20 minutes.

The third component is the *sample holder*. Samples subjected to analysis are held in sample pans made of platinum, aluminum, or alumina. Platinum is most often used because of its inertness and ease of cleaning. Sample pan volumes range from 40 μL to 500 μL.

Due to several problems such as potential contamination of samples or their catalytic decomposition, temperatures are generally measured with a small thermocouple located as close as possible to the sample container. The temperatures recorded can generally lag or lead the actual sample temperature. In modern TGA systems, a computerized temperature control routine is used. It automatically compares the voltage output of the thermocouple with a voltage-versus-temperature table stored in the computer memory. The computer utilizes the difference between the temperature of the thermocouple and the temperature specified to adjust the voltage to the heater. Sometimes, the same thermocouple behaves as the heating element and temperature sensor simultaneously. Using modern control systems, it is possible to achieve excellent agreement between the specified temperature program and temperature of the sample. Typically, the reproducibility of measurement for a particular program falls within 2 ^{o}C throughout an instrument's operational range.

Since TGA monitors the mass of the analyzed sample with temperature, the information obtained is quantitative. There are some limitations, such as decomposition and oxidation reactions; physical processes as vaporization, sublimation, and desorption. However, compositional analysis and decomposition profiles are among the most important applications of TGA. For polymeric systems, thermograms provide information on decomposition mechanisms for various decomposition preparations. The uniqueness of polymer thermal decomposition pattern can be used sometimes for identification purposes.

We utilized TGA to examine the thermal stability of copolymer samples prior to DSC analysis.

Differential Scanning Calorimetry (DSC) is the most frequently used thermal analysis method because of its availability, simplicity and speed. Instruments for DSC contain a sample holder and reference. Heaters either ramp or hold the given temperature. The instrument measures the difference between the sample and reference in the heat flow. There are three different types of DSC instruments: *power-compensated DSC, heat-flux DSC, and modulated DSC.*

Power-compensated DSC is based on holding the sample and reference temperatures equal, while both temperatures are increased or decreased linearly. The instrument measures the power needed to maintain the sample temperature equal to the reference temperature. This technique has lower sensitivity in comparison with heat-flux DSC, but its response time is faster.

The heat-flux DSC relies on the difference in heat flow into the sample and reference, while the sample temperature is changed at constant rate. The heating unit is

the same for both sample and reference. We can write the total heat flow for the heat-flux DSC as:

$$\frac{dH}{dt} = C_p \frac{dT}{dt} + f(T, t) \tag{1.1}$$

where, H is the enthalpy in J/mol, C_p is the specific heat capacity in J/(K·mol), and f(T, t) is the kinetic response of the sample in J/mol. The total heat flow is the sum of two terms, one related to the heat capacity, and the other related to the kinetic response. Several processes occur as the temperature is changed: a decrease in the heat flow represents an endothermic process, while an increase in heat flow represents an exothermic process (*Figure 1.2.1*).

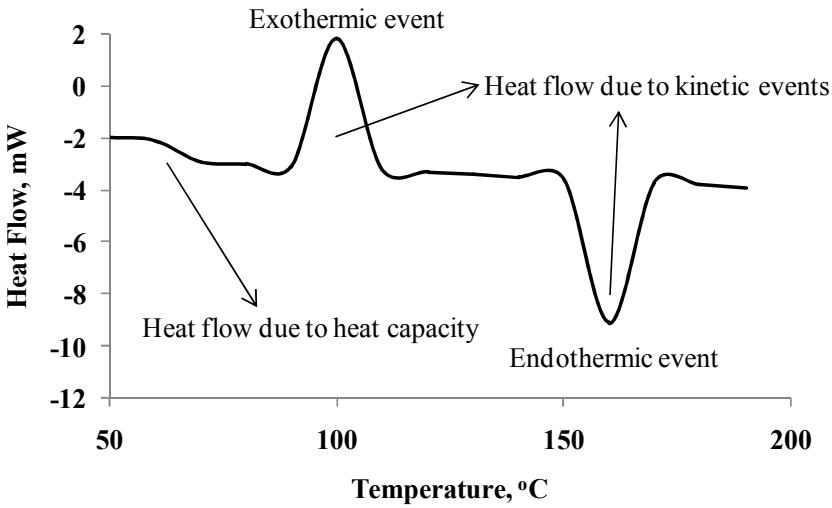

Figure 1.2.1. Typical DSC scans for a polymeric material.

In *Modulated DSC*, the same heating and cell arrangements are utilized. In the analysis a sinusoidal function is superimposed on the overall temperature program to produce a micro heating and cooling cycle, as the overall temperature is steadily increased or decreased. Using Fourier Transform methods, the overall signal is split up into two parts: a reversing heat flow signal and a non-reversing heat flow signal. The first one is associated with the heat capacity component of the thermogram, and the second one is related to kinetic processes. Normally, exothermic and endothermic events may appear in either one or both heat flow signals, while the step transitions, such as glass transition temperature, appear only in the reversing signal.

Modern Differential Scanning Calorimetric instruments are equipped with custom software, which is available to aid the user in determining melting points, glass transition temperatures and heat capacity values. The temperatures of step transitions and kinetic events are normally determined as onset temperatures. This is defined as the temperature

at which a tangent to the baseline intersects the tangent to the slope of the transition. Sometimes, the glass transition temperature is taken as the midpoint of the transition rather than the onset. The enthalpy of melting or crystallization is determined by integration of the representative peak on endotherm or exotherm.

DSC is used widely for examining polymers transitions and to check their composition. Melting points and glass transition temperatures for most polymers are available from standard compilations, and the method can show possible polymer degradation by the lowering of expected melting point. T_m depends on the molecular weight of the polymer. The percentage crystallinity of a polymer can also be obtained using DSC.

We used the Heat-Flux DSC to examine the thermal properties of copolymers in bulk. We monitored the fusion\crystallization temperatures and enthalpies as a function of AA incorporation.

High Sensitivity DSC. This method is based on the same principle as the conventional DSC, measuring the heat absorbed or released as a function of temperature.

$$\frac{dQ_p}{dt}\frac{1}{\sigma M} = C_p \tag{1.2}$$

where σ is the scan rate dT/dt; T is the temperature; M is the number of moles of sample in the sample cell.

The HS-DSC instrumentation has sensitivity of approximately 100 μV/mW and a calorimetric precision near +/-0.1 % (VP-DSC)[64]. This technique provides information on thermodynamic parameters associated with the heating/cooling of the targeted object (polymer) *in solution*. Particularly, the change of heat capacity at constant pressure is

measured as a function of temperature. It is also possible to calculate the change in enthalpy or entropy, and phase transition temperature.

$$\Delta H = \int_{T<T_m}^{T>T_m} \Delta C_p \, dT = \Delta C_p \, (T_{T>T_m} - T_{T<T_m}) \quad (1.3)$$

$$\Delta S = \int_{T<T_m}^{T>T_m} \frac{\Delta C_p}{T} \, dT = \Delta C_p \, \ln(T_{T>T_m} - T_{T<T_m}) \quad (1.4)$$

where $T<T_m$ and $T>T_m$ represents the region of temperature before and after phase transition temperature T_m respectively.

This technique we used to examine the thermoresponsive behaviour of nanoparticles in colloidal solution.

1.2.2 X-ray Powder Diffraction[65-67]

X-ray Powder Diffraction (XrPD) is an analytical technique used to identify the phase constitution of a crystalline material and can provide information about unit cell dimensions. The main basics were laid by Max von Laue in 1912 when he discovered that crystalline material can act as a grating for the X-ray wavelength. A powdered sample normally contains each possible crystalline orientation of initial sample. 3D reciprocal space can be generated by the orientational averaging and is studied by the projection onto a single dimension. The generated 3D space can be described with axes such as **x′, y′**and **z′**or by the other approach through spherical coordinates **q, φ′, χ′**. In powder diffraction, the intensity appears as homogeneous over **φ′** and **χ′** and only **q** remains as an important measurable quantity.

The scattering and collection of the radiation behind the sample plane results in smooth diffraction rings on a flat detector's plate as well as Laue spots, observable during single crystal diffraction. The beam axis is the height of the imaginary cone with bottom formed from a ring, generated on detector's surface.

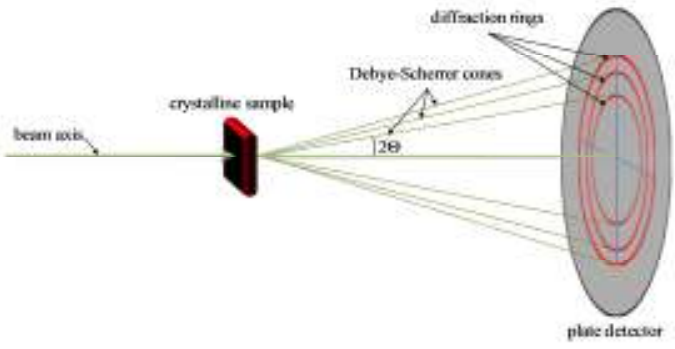

Figure 1.2.2. X-ray powder diffraction: basic experimental setup.

The angle between the beam axis and the ring normal is called "scattering angle" denoted as 2θ. According to the Bragg relation, each ring corresponds to a particular reciprocal lattice vector *G* in the sample crystal, denoted as:

$$G = q = 2k' \sin(\theta) = \frac{4\pi \sin(\theta)}{\lambda} \quad (1.5)$$

where ***k'*** is the wave vector and $\boldsymbol{\lambda}$ is the wavelength. The Bragg's law is:

$$n\lambda = 2d \sin(\theta) \quad (1.6)$$

where ***d*** is the lattice spacing and ***n*** is an integer of the incident wavelength (normally equals to 1). X-ray powder diffraction data are usually obtained as a *diffractogram* where the diffracted intensity ***I*** is shown as a function of the scattering angle 2θ or as a function of the d spacing.

In contrast to crystalline materials, amorphous ones generate wide background signal. There appears an apparent difference between small or low molecular weight molecules and long chain polymers. In the case of long chain polymers, the complete crystalline structure is never reached, because the surfaces of folded chains, chain ends and other structural disarrangements always constitute the amorphous phase. The terms "semi-crystallinity" and "degree of crystallinity" are frequently used to define the fraction of the crystalline phase in the total mass. The results on degree of crystallinity obtained from the XrPD may be comparable with those of other methods such as DSC only in the case of simple systems such as homopolymers of diblock copolymers.

This technique we used to examine the crystallinity percentages of copolymer samples. In addition, we used it to determine the type of elementary unit cell in polyethylene crystallites.

1.2.3 Infrared Spectroscopy[62]

Fourier Transform Infrared Spectroscopy can be used to reveal the formation the extensive hydrogen bond network in the powder samples of copolymers, which contain active H-H donor/acceptor groups, such as carboxylic acid, amine, esters, etc. Additionally, the use of FTIR spectrometry in assessment of functional group protection removal (usually, by hydrolysis) completeness and in estimation of percentage of these functional groups, involved into H-H bond network might be very useful and informative.

In our studies, we used FTIR for detecting hydrogen-bonded carboxylic dyads, formed in bulk copolymer samples. The carboxylic group is represented by two distinctive infrared stretching absorptions. These two absorptions have a notable change upon hydrogen bonding. The first one, the O-H stretching absorption for carboxylic dimers is very strong and broad, extending from 2500 to 3300 cm^{-1}. This absorption overlaps with broad C-H stretching peaks of pE at 3000-3300 cm^{-1} and it may not be clearly seen. The –C-O-H "in plane" bend of the monomeric carboxylic acid group is found at 1410-1420 cm^{-1}. When the carboxylic acid dimer is formed, the –O-H "out-of-plane" bend appears at 930-940 cm^{-1}. Second characteristic absorption, the stretching frequency of the carboxylic group monomer is found near 1700-1710 cm^{-1}. This frequency is increased to 1740-1750 cm^{-1} when carboxylic group contributes to the hydrogen-bended dimer.

Such kind of combined analysis presents a powerful tool in understanding of the polymers microphase organization in bulk. These properties are important in further processing of the copolymers.

1.2.4 Nuclear Magnetic Resonance Spectroscopy[68]

Quantitative structural analysis is important and very effective in the study of homopolymers as well as multicomponent copolymers (di-, tri- and more components; block or random). High-resolution NMR spectroscopy provides information on sequence and structural details, which are impossible to determine by other techniques. The composition of the copolymer can be determined very easily by proton (^{1}H) NMR and this method is much more accurate than any other available analytical method, such as elemental analysis.

In conventional ^{1}H NMR, copolymer compositions are usually determined by the ratio between relative intensities of the chosen group proton peaks, such as $–CH_3$ protons in tertiary-butyl acrylate ester or –CH- proton in free acrylate. These groups are unprotected and protected forms respectively of the carboxylic functional group in pE-co-AA copolymers.

Copolymer properties depend not only on its composition, but also on comonomer sequence. The comonomer dyads, triads and even tetrads can be distinguished by the character of peak splitting of the certain protons or carbons in ^{1}H and carbon- (^{13}C) NMR spectrum.

In the case when a copolymer contains prochiral monomers, the configurational sequences must be considered also and there are sets of sequences for dyads and triads. The sequences number in n-ads increases largely with *n*.

We utilized the current technique in determination of molar percentages of AA in copolymer samples. We used it to prove the successfulness of TBA to AA conversion after hydrolysis.

1.2.5 Dynamic Light Scattering[62,69,70]

Dynamic light scattering is a physical technique, which can be utilized to determine the size distribution data of suspended small particles or polymer molecules in solution. The technique can also be used to study the behavior of complicated complex fluids such as concentrated polymer solutions.

In the case where the light strikes small particles, the particles are transformed into individual all directional light scattering centers (Rayleigh scattering) as long as the particles are small enough compared to the wavelength (below 250nm). When the incident light is produced by a laser and it is coherent and monochromatic, we can observe a time-dependent fluctuation in the scattering intensity. The observed fluctuations are due to the Brownian motion of the small molecules in solution and so the distance which separates the scatterers is changing with time. The light which was already scattered is subjected to either constructive or destructive interference by the surrounding particles and intensity fluctuation contains the information about the time scale of scatterers' movement. There exist various ways to acquire dynamic information about particles' movement in solution by Brownian motion. One of them is dynamic light scattering or quasi-elastic laser light scattering technique. In this technique, the intensity trace of an autocorrelation function is recorded during the experiment. This trace contains data about the dynamic information of the particles. The autocorrelation function (second order) is derived from the trace of intensity as follows:

$$g^2(q;\tau) = \frac{[I(t)I(t+\tau)}{[I(t)]^2} \tag{1.7}$$

where $g^2(q;\tau)$ is the autocorrelation function at a particular wave vector, q, and delay time, τ, and I is the intensity. At the start, the correlation appears to be high due the impossibility of the particles to move very far from their primary position. Because of that, the two signals are almost unchanged when compared after only a very short time interval. As the time delays become longer, the exponential growth of the correlation starts to be observed. This change means that after long periods of time, the correlation between the scattered intensity of the initial and final states vanishes. The exponential component is related to the diffusion coefficient, i.e. to the motion of the particles. Normally, the autocorrelation function is fitted and a number of methods could be used for this purpose. These methods are normally based on calculations of assumed distributions. In the case with a monodisperse sample, the decay function is a single exponential. The second order autocorrelation function is dependent on the first order autocorrelation function $g^1(q;\tau)$ as follows:

$$g^2(q;\ \tau) = 1 + \beta\ [g^1(q;\ \tau)]^2 \tag{1.8}$$

where the parameter β is a correction factor. This parameter is related to the alignment and geometry of the laser beam in the basic light scattering setup. Approximately, this parameter is equal to the number of spots, from which light is collected. The main application of the autocorrelation function is the size determination procedure.

Dynamic Light Scattering data analysis. Once the autocorrelation data have been generated, different mathematical approaches can be employed to interpret them. Multiple mathematical approaches are possible to employ for the interpretation of the collected autocorrelation data. The analysis of the scattering data is easy when the

interactions between particles are minimized. The interaction through collisions or electrostatic forces can be depressed by dilution, and charge effects are possible to reduce by the use of salts.

The treatment of the first order autocorrelation function as a single exponential decay is the easiest approach. It is possible to use when the population is monodisperse.

$$g^1(q;\,\tau) = \exp(-\Gamma\tau) \tag{1.9}$$

where $\boldsymbol{\Gamma}$ is the decay rate. It is possible to derive the translational diffusion coefficient $\boldsymbol{D_t}$ at a single angle or at a range of angles depending on the wave vector $\boldsymbol{q}$:

$$\Gamma = q^2 D_t \tag{1.10}$$

with the relation for $\boldsymbol{q}$:

$$q = \frac{4\pi n_0}{\lambda}\sin\left(\frac{\theta}{2}\right) \tag{1.11}$$

where $\boldsymbol{\lambda}$ is wavelength of the incident laser, $\boldsymbol{n_0}$ is the refractive index of the sample and $\boldsymbol{\theta}$ is angle between detector and sample cell.

The parameters of anisotropy and polydispersity may influence the angular dependency of the resultant plot of $\boldsymbol{\Gamma/q^2}$vs.$\boldsymbol{q^2}$. If particles are small and spherical in shape, no angular dependence as well as anisotropy will be shown. Thus, the horizontal line will be the result for the $\boldsymbol{\Gamma/q^2}$ vs. $\boldsymbol{q^2}$ plot. When the morphology of particles is different, the system anisotropy will appear and thus an angular dependence will take place, when plotting of $\boldsymbol{\Gamma/q^2}$ vs. $\boldsymbol{q^2}$ ($\boldsymbol{D_t}$. is the intercept).

The calculation of the hydrodynamic radius of the sphere involves $\boldsymbol{D_t}$ through the Stokes-Einstein equation:

$$D_t = \frac{k_B T}{3\pi\eta d} \tag{1.12}$$

This relation gives the size of the sphere that is moving in the same fashion as the scatterer. For example, the determined hydrodynamic radius for the random coil of the polymer in solution is not the same as the radius of gyration, found by static light scattering. The determined size will include the contributions from other molecules or solvent molecules, which move simultaneously with the particle. So, the sum of the exponential decays of each of the species in the population yields the autocorrelation function.

$$\sum_{i=1}^{n} G_i(\Gamma_i) \exp(-\Gamma_i \tau)\, d\Gamma = \int G(\Gamma) \exp(\Gamma\tau)\, d\Gamma = g^1(q;\, \tau) \qquad (1.13)$$

Very interesting results may be obtained for $\boldsymbol{g^1(q;\, \tau)}$, if one will invert this relation and extract $\boldsymbol{G(\Gamma)}$. This component contains the information on size distribution which is proportional to the relative partial scattering from the species. The following methods are used in the autocorrelation function interpretation.

Cumulant method. Besides the sum of exponentials, information on the variance of the system is obtained from the method as follows:

$$g^1(q,\tau) = exp\big(-\overline{\Gamma}\tau\big)\left(1 + \frac{\mu_2}{2!}\tau^2 - \frac{\mu_3}{3!}\tau^3 + \cdots\right) \qquad (1.14)$$

where $\overline{\Gamma}$ is the average decay rate and $\frac{\mu^2}{\overline{\Gamma}^2}$ is the second order polydispersity index (or an indication of the variance). Also, there is a possibility to derive a third order polydispersity index, but this procedure is necessary only when the studied objects are very polydisperse. The *z*-averaged diffusion coefficient $\boldsymbol{D_z}$ can be obtained at one or at the range of angles depending on the wave vector $\boldsymbol{q}$.

$$\overline{\Gamma} = q^2 D_z \qquad (1.15)$$

The cumulant method is appropriate for small $\boldsymbol{\tau}$ and considerably narrow $\mathbf{G(\Gamma)}$. As an advantage it is necessary to note, that the cumulant method is not affected by experimental noise as opposed to the CONTIN algorithm or Maximum entropy methods.

CONTIN algorithm. This method relies on the analysis of the autocorrelation function through an inverse Laplace transform. The method was developed by Steven Provencher[71,72]. Cumulant method is not suitable for characterization of heterodisperse, polydisperse or multimodal systems, while the CONTIN algorithm provides the resolution for separating two different particle populations of approximately a factor of five or higher and the difference in relative intensities between two different populations should be less than $1{:}10^{-5}$.

Maximum entropy method. The maximum entropy method includes a number of multiple steps to minimize the deviation of the fitted data from the experimental data and subsequently reducing the $\boldsymbol{\chi^2}$of the fitted data.

Interpretation of the DLS data in the case of non-spherical, elongated objects. Since the conventional interpretation of the DLS data in terms of the diffusion coefficient provides an assumption, that scatterers of light (nanoparticles) are hard spheres, the results for non-spherical objects will appear very different. In other words, the hydrodynamic radius of non-spherical particles is not equal to their geometrical radius. The hydrodynamic radius is derived from the self-diffusion coefficient via the equation (15) and for an elongated particle of length **L** and cross-section **d** in water of viscosity $\boldsymbol{\eta}$ at a temperature **T**, can be expressed as:

$$\mathrm{D} = \left(\frac{\mathrm{k_B T}}{3\pi\eta \mathrm{L}}\right)\left(\ln \mathrm{p} + 0.312 + \frac{0.565}{\mathrm{p}} - \frac{0.100}{\mathrm{p}^2}\right) \tag{1.16}$$

where p = L/d.[73,74] The Stokes-Einstein formula ($D = k_BT/6\pi\eta R_h$) can then be used to calculate a hydrodynamic radius R_h. Normally, the values obtained by this approach are in good agreement with those obtained by imaging techniques (where geometrical parameters of the nanoparticles are directly measured).

We used DLS analysis to examine the hydrodynamic radius (R_H) of copolymer nanoparticles in colloidal solution. Additionally, we applied the heating protocol to colloidal solutions to monitor R_H as a function of temperature.

1.3 References

1. von Pechmann, H. *Ber. Dtsch. Chem. Ges.* **1989**, *31*, 2640-2646.
2. Bamberger, E.; Tschirner, F. *Ber. Dtsch. Chem. Ges.* **1900**, *33*, 955-959.
3. Carothers, W. H.; Hill, J. W.; Kirby, J. E.; Jacobson, R. A. *J. Am. Chem. Soc.* **1930**, *52*, 5279-5288.
4. Friedrich, M. E. P.; Marvel, C. S. *J. Am. Chem. Soc.* **1930**, *52*, 376-387.
5. Koch, H.; Ibing, G. *Brennst.-Chem.* **1935**, *16*, 141-148.
6. Fawcett, E. W. G., R.O. *J. Am. Chem. Soc.* **1934**, 368-395.
7. Fawcett, E. W.; Gibson, R. O.; Perrin, M.; Patton, E. G.; Williams, E. G. *Brit. Patent 2816883,* **Sep. 6, 1937,** *Imperial Chemical Industries, Ltd.*
8. Hogan, J. P.; Banks, R. L. **1958,** *US Patent 2825721*.
9. Hogan, J. P. *J. Polym. Sci.* **1970**, *8*, 2637-2652.
10. Clark, A. *Catal. Rev.* **1969**, *3*, 145-149.
11. McDaniel, M. P. *Ind. Eng. Chem. Res.* **1988**, *27*, 1559-1564.
12. Weckhuysen, B. M.; Schoonheydt, R. A. *Catalysis Today,* **1999**, *51*, 215-221.
13. Ziegler, K.; Holtzkamp, E.; Martin, H.; Breil, H. *Angew. Chem.* **1955**, *67*, 541-547.
14. Ziegler, K.; Holtzkamp, E.; Martin, H.; Breil, H. *Angew. Chem.* **1955**, *67*, 426-429.
15. Natta, G. *J. Polym. Sci.* **1955**, *16*, 143-154.
16. Natta, G. *Angew. Chem.* **1956**, *68*, 393-397.
17. McDaniel, M. P. *Adv. Catal.* **1985**, *43*, 43-47.

18. Gardner, K.; Parsons, I. W.; Hawward, R. N. *Polym. Sci., Part A: Polym. Chem.* **1978**, *16*, 1683-1696.

19. Kealy, T. J.; Pauson, P. L. *Nature,* **1951**, *168*, 1039-1040.

20. Sinn, H.; Kaminsky, W. *Adv. Organomet. Chem.* **1980**, *18*, 99-104.

21. Paquette, L. A.; Moriarty, K. J.; Meunier, P.; Gautheron, B.; Sornay, C.; Rogers, R. D.; Rheingold, A. L. *Organometallics,* **1989**, *8*, 2159-2167.

22. Charpentier, P. A.; Zhu, S.; Hamielec, A. E.; Brook, M. A. *Ind. Eng. Chem. Res.* **1997**, *36*, 5074-5082.

23. Johnson, L. K.; Killian, C. M.; Brookhart, M. *J. Am. Chem. Soc.* **1995**, *117*, 6414-6415.

24. Rix, F. C.; Brookhart, M. *J. Am. Chem. Soc.* **1995**, *117*, 1137-1138.

25. Johnson, L. K.; Mecking, S.; Brookhart, M. *J. Am. Chem. Soc.* **1996**, *118*, 267-268.

26. Baugh, L. S.; Sissano, J. A.; Kacker, S.; Berluche, E.; Stibrany, R. T.; Schulz, D. N.; Rucker, S. P. *J. Polym. Part A: Polym. Chem.* **2006**, *44*, 1817-1840.

27. Drent, E.; van Dijk, R.; van Ginkel, R.; van Oort, B.; Pugh, R. I. *Chem. Comm.* **2002**, *2002*, 744-745.

28. Goodall, B. L.; Grubbs, R. H.; Waltman, A. W. US 2005215738 A1. *U.S. Patent Application.* **2005**, *Publ. Rohm and Haas Company*,

29. Leung, D. H.; Ziller, J. W.; Guan, Z. *J. Am. Chem. Soc.* **2008**, *130*, 7538-7539.

30. Luo, S.; Vela, J.; Lief, G. R.; Jordan, R. F. *J. Am. Chem. Soc.* **2007**, *129*, 8946-8947.

31. Michalak, A.; Ziegler, K. *Organometallics,* **2001**, *20*, 1521-1532.

32. Nagel, M.; Sen, A. *Organometallics,* **2006**, *25*, 4722-4724.

33. Sen, A.; Borkar, S. *J. Organometal. Chem.* **2007**, *692*, 3291-3299.

34. Waltman, A. W.; Grubbs, R. H. *Organometallics,* **2004**, *23*, 3105-3107.

35. Waltman, A. W.; Ritter, T.; Grubbs, R. H. *Organometallics,* **2006**, *25*, 4238-4239.

36. Waltman, A. W.; Younkin, T. R.; Grubbs, R. H. *Organometallics,* **2004**, *23*, 5121-5123.

37. Wang, C.; Friedrich, S.; Younkin, T. R.; Li, R. T.; Grubbs, R. H.; Bansleben, D. A.; Day, M. W. *Organometallics,* **1998**, *17*, 3149-3151.

38. McLain, S. J.; Sweetman, K. J.; Johnson, L. K.; McCord, E. *Polym. Mater. Sci. Eng.* **2002**, *86*, 320-321.

39. Goodall, B. L. *Topics in Organomet. Chem.,* **2010**, *DOI: 10. 1007 / 3418,* **2008,** *6*, 1-20.

40. Carnacho, D. H.; Salo, E. V.; Ziller, J. W.; Guan, Z. *Angew. Chem. Intl. Ed.* **2004**, *43*, 1821-1827.

41. Popeney, C. S.; Guan, Z. *Organometallics,* **2005**, *24*, 1145-1155.

42. Popeney, C. S.; Camacho, D. H.; Guan, Z. *J. Am. Chem. Soc.* **2007**, *129*, 10062-10063.

43. Younkin, T. R.; Connor, E. F.; Henderson, J. L.; Friedrich, S. K.; Grubbs, R. H.; Bansleben, D. A. *Science,* **2000**, *297*, 460-461.

44. Michalak, A.; Ziegler, K. *J. Am. Chem. Soc.* **2001**, *123*, 12266-12278.

45. Connor, E. F.; Younkin, T. R.; Henderson, J. L.; Waltman, A. W.; Grubbs, R. H. *Chem. Commun.* **2003**, *2003*, 2272-2273.

46. Ito, S.; Nozaki, K. *The Chemical Record,* **2010**, *10*, 315-325.

47. Behr, A.; Keim, W. *Arabian J. Sci. Eng.* **1985**, *10*, 377-390.

48. Allen, N. T.; Goodall, B. L.; McIntosh, L. H. *U.S. Patent Application. US 20070049712 A1,* **2005***, Publ. Rohm and Haas Company*.

49. Weng, W.; Shen, Z.; Jordan, R. F. *J. Am. Chem. Soc.* **2007**, *129*, 15450-15451.

50. Skupov, K. M.; Piche, L.; Claverie, J. P. *Macromolecules,* **2008**, *41*, 2309-2310.

51. Skupov, K. M.; Marella, P. R.; Hobbs, J. L.; McIntosh, L. H.; Goodall, B. L.; Claverie, J. P. *Macromolecules,* **2006**, *39*, 4279-4281.

52. Bae, C.; Hartwig, J. F.; Harris, N. K. B.; Long, R. O.; Anderson, K. S.; Hillmyer, M. A. *J. Am. Chem. Soc.* **2005**, *127*, 767-776.

53. Lehman Jr., S. E.; Wagener, K. B.; Baugh, L. S.; Rucker, S. P.; Schulz, D. N.; Varma-Nair, M.; Berluche, E. *Macromolecules* **2007**, *40*, 2643-2656.

54. Yang, H.; Islam, M.; Budde, C.; Rowan, S. J. *J. Polym. Part A: Polym. Chem.* **2003**, *41*, 2107-2116.

55. Lehman, S. E., Jr.; Wagener, K. B.; Baugh, L. S.; Rucker, S. P.; Schulz, D. N.; Varma-Nair, M.; Berluche, E. *Macromolecules* **2007**, *40*, 2643-2656.

56. Seitz, M. E.; Chan, C. D.; Opper, K. L.; Baughman, T. W.; Wagener, K. B.; Winey, K. I. *J. Am. Chem. Soc.* **2010**, *132*, 8165-8173.

57. Berda, E. B.; Wagener, K. B. *Macromolecules* **2008**, *41*, 5116-5122.

58. Breitenkamp, K.; Junge, D.; Emrick, T. *Polymeric Drug Delivery I* **2006**, *18*, 253-267.

59. Brown, M. E. *Introduction to Thermal Analysis*, Dordrecht, The Netherlands: Kluwer Academic Publishers, **2001**, p. 264.

60. Earnest, C.M. (Ed.), *Compositional Analysis by TG*, Philadelphia, US: ASTM International, **1987**, p. 293.

61. Wunderlich, B. *Thermal Analysis of Polymeric Materials*, Dordrecht, The Netherlands: Springer-Verlag Berlin Heidelberg, **2005**, p. 894.

62. Skoog, D. A.; Holler, F. J.; Crouch, S. R. *Principles of Instrumental Analysis, 6th Edition,* Canada: Thomson-Brooks/Cole, **2007**, p. 1039.

63. *VP-DSC Microcalorimeter User's Manual*.

64. Pecharsky, V. K.; Zavalij, P. Y. *Fundamentals of Powder Diffraction and Structural Characterization of Materials*, New York, US: Springer Science+Busyness Media, **2009**, p. 741.

65. Warren, B. E. *X-ray Diffraction,* New York, US: Courier Dover Publications, **1990**, p. 381.

66. Will, G. *Powder Diffraction,* Würzburg, Germany: Springer-Verlag Berlin Heidelberg, **2006**, p. 224.

67. Hatada, K.; Kitayama, T. *NMR Spectroscopy of Polymers*, Wurzburg, Germany: Springer-Verlag Berlin Heidelberg, **2004**, p. 222.

68. Pecora, R.; Berne, B. *Dynamic Light Scattering with Applications to Chemistry, Biology and Physics,* Toronto, CA: Courier Dover Publications, **2000**, p. 376.

69. Xu, R. *Particle Characterization: Light Scattering Methods,* Dordrecht, The Netherlands: Kluwer Academic Publishers, **2000**, p. 397.

70. Provencher, S. W. *Comp. Physics Comm.* **1981**, *27*, 213-227.

71. Provencher, S. W. *Comp. Physics Comm.* **1982**, *27*, 229-242.

72. Pecora, R. *J. Nanopart. Res.* **2000**, *2*, 123-131.

73. Tirado, M. M.; Martinez, M. C. L.; Torre, J. G. d. l. *J. Chem. Phys.* **1979**, *71, 2581-2587*.

CHAPTER II

Research article:

«Amphiphilic polyethylenes leading to surfactant-free thermoresponsive nanoparticles»

Authors:

Vladimir A. Kryuchkov[1], Jean-Christophe Daigle[2], Kirill M. Skupov[1,2],

Jerome P. Claverie[2] and Françoise M. Winnik[1]

Published:

Journal of American Chemical Society, 2010, 132 (44), pp 15573–15579
Publication Date (Web): October 14, 2010
Publication Date (Issue): November 10, 2010

2.1 Abstract

Linear copolymers of ethylene and acrylic acid (PEAA) were prepared by catalytic polymerization of ethylene and *tert*-butyl acrylate followed by hydrolysis of the ester groups. The copolymers contained COOH groups inserted into the crystalline unit cell with formation of intramolecular hydrogen-bonds, as established on the basis of differential scanning calorimetry (DSC), Fourier-transform infrared spectroscopy (FTIR), and X-ray diffraction (XRD) studies. A solvent-exchange protocol, with no added surfactant, converted a solution in tetrahydrofuran of a PEAA sample containing 12 mol% of acrylic acid (AA) into a colloidally stable aqueous suspension of nanoparticles. Transmission electron microscopy (TEM), dynamic light scattering (DLS), and high sensitivity differential scanning calorimetry (HS-DSC) were used to characterize the nanoparticles. They are single crystals of elongated shape with a polar radius of 49 nm (σ = 15 nm) and an equatorial radius of 9 nm (σ = 3 nm) stabilized in aqueous media via carboxylate groups located preferentially on the particle/water interface. The PEAA (AA: 12 mol%) nanoparticles dispersed in aqueous media exhibited a remarkable reversible thermoresponsive behavior upon heating/cooling from 25 to 80 °C.

2.2 Introduction

Polymeric nanoparticles are the focus of intensive research in view of their numerous applications in areas such as nanomedicine,[1-4] imaging,[5,6] diagnostics,[7] chemical separations,[8,9] sensors,[8] catalysis,[10,11] and colloidal crystals.[12] They are obtained by self-assembly of copolymers consisting of hydrophobic and hydrophilic fragments, or amphiphilic copolymers. There exist currently a plethora of such polymers with various degrees of structural complexity, which are synthesized by all types of polymerizations and also obtained by modification of natural polymers. Yet, only a few nanoparticles based on amphiphilic copolymers of ethylene have been reported to date. Copolymers of ethylene and hydrophilic charged monomers are well-known as typical examples of ionomers, which are thermoplastic polymers that contain a small fraction of pendant ionic functional groups.[13] For instance, random copolymers of ethylene and methacrylic acid, approximately 85:15 mol:mol, where some of the acid groups are converted to metal salts, are commercially important polymers extensively used in a variety of applications, including orthodics and prosthetics, as films, adhesive layers in foil/paper containers, and as constituents of items such as golf balls and bowling pins. In bulk, they contain amorphous and crystalline polyethylene phases as well as ionic clusters acting as physical crosslinks.[13,14] The introduction of the ionic groups greatly improves the mechanical and optical properties of the copolymers. A limited number of studies of ionomers in water were carried out in the late 1990's, especially by the group of Schlick, who probed the microstructure of polymeric micelles formed in aqueous solutions of poly[ethylene-co-(potassium methacrylate)] with 7.5 mol % methacrylate (Mn = 20,500 g/mol, PDI = 4).[15,16] Using fluorescence and electron spin resonance spectroscopy, they determined

that the particles have an amorphous core formed by the hydrophobic PE fragments surrounded by an external shell in which the polar groups are concentrated. A new class of amphiphilic polyolefins prepared by metathesis,[17-19] the so-called precision polyolefins, where the polar substituents are always separated by the same number of methylene groups, are expected to show interesting properties in aqueous media, but the study of their self-assembly is still in its infancy.[20] Emrick *et al.* have reported recently a preparation, by ring-opening metathesis polymerization, of amphiphilic polyolefins bearing a wide range of polar groups.[20-22] Phosphorylcholine-substituted polyolefins were shown to self-assemble in water into stable "polymersomes", which are promising biomimetic materials.[23] Polymers of this type are amorphous and soluble in organic solvents at room temperature. Hence, they differ greatly from conventional polyolefins, which are crystalline and insoluble in any organic solvent at room temperature.

From a mechanistic view point, the self assembly in water of crystalline PE bearing polar groups presents fascinating aspects, since it is expected to be directed not only by the balance between hydrophilic and hydrophobic interaction energies, but also by the propensity of PE to crystallize, in contrast to the situation with amorphous amphiphilic polymers. The crystallization driving force may, in fact, be critical, if one judges from recent reports from the group of Mecking on the formation of pure PE nanoparticles (~ 10 nm) upon catalytic polymerization of ethylene in water using water-soluble catalysts and surfactants.[24] The core of the nanoparticles consists of single lamella hexagonal PE crystals of narrow size distribution and thickness (6.3 nm). The nanoparticles[25] owe their stability in water to the presence of a surfactant shell acting as colloidal stabilizer. A study by Li *et al.* of the self-assembly in water of linear poly(ethylene-b-ethylene oxide)

also points to the importance of the tendency of PE towards crystallization.[26] In water at room temperature polyethylene-*b*-poly(ethylene oxide) copolymers form multicore micelles believed to result from the aggregation of smaller single core polymeric micelles with a crystalline central PE phase.

Crystalline PE is readily prepared by catalytic polymerization of ethylene. However, the insertion of polar comonomers along the polyethylene (PE) backbone by catalytic polymerization constitutes a considerable synthetic challenge, since polar functional groups interfere with the catalytic process via various deactivation processes.[27] Nonetheless, over the last decades important progress has been made towards achieving the catalytic *s*ynthesis of linear ethylene copolymers containing polar functionalities.[27] Several synthetic routes have been reported, yielding polymers bearing pendant esters,[28-30] nitriles, [31] amides, [32] N-carboxyl groups[32] and ether groups.[33] We report here the first preparation by catalytic polymerization of linear crystalline ethylene *tert*-butyl acrylate (TBA) random copolymers with various degrees of acrylate incorporation. These copolymers are readily converted to the corresponding poly(ethylene-co-acrylic acid) (PEAA) (Scheme 1), which are excellent candidates for testing the impact of the driving force towards crystallization on the self assembly of amphiphilic polymers. We used a room temperature, surfactant-free solvent-exchange method to trigger the self-assembly in neutral (pH 7) water of PEAA samples.

This process yielded crystalline nanoparticles of remarkable colloidal stability in water over a wide range of temperatures and pHs. We also describe how the level of AA incorporation along the PE chains directs the copolymer self-assembly in water and we examine the influence of crystallinity on the process. Finally, we demonstrate, using

high-sensitivity microcalorimetry and dynamic light scattering, that the colloidal aqueous PEAA nanoparticles exhibit a reversible thermosensitivity driven by the fusion/crystallization of their polyethylene core. To our knowledge, this is the first time that thermosensitivity is observed for a colloidal polyolefin.

2.3 Experimental Section

2.3.1 General Methods and Materials

All polymerizations were performed under argon using standard Schlenk techniques. The catalyst, MePd(pyridine)P(-3-Me-6-SO_3-C_6H_3)$(Ph)_2$, was prepared according to a literature procedure.[1] Toluene for polymerization was purified by distillation over CaH_2 and degassed using three freeze pump thaw cycles and kept over activated molecular sieves. Research grade ethylene (Praxair) was purified over an O_2 scavenger trap prior to use. *Tert*-butyl acrylate (TBA, Aldrich) was purified by sparging it with argon, and passing it over a bed of inhibitor remover resin (Aldrich). It was then spiked with *tert*-butyl catechol (0.25% wt:wt). All other chemicals were purchased from Sigma Aldrich, except for deuterated solvents which were obtained from CDN Isotopes.

NMR spectra were recorded on a Varian Inova 600MHz spectrometer. For ^{13}C spectra (5000 scans), an ungated decoupling sequence with a pulse angle of 20^o and a delay of 10s between two scans was used in order to ensure quantitative measurements. FTIR spectra were recorded on a Nicolet 6700 Spectrometer equipped with Smart ATR accessory (ThermoSci). Differential scanning calorimetry measurements (DSC) of solid samples were performed on a DSC823e (TOPEM modulation) equipped with an FRS5 sample cell, a sample robot, a Julabo FT400 intracooler and an HRS7 sensor from Mettler Toledo. Samples were heated from 20^oC to 140^oC at a rate of 0.3 ^oC/minute and data were analyzed with STAR software. The amplitude of TOPEM modulation was 0.025K, using switching times comprised between 15 and 30 seconds. All reported values are for samples, which have been slowly cooled from the melt at a rate of 0.3 ^oC/minute.

2.3.2 Preparation of poly(ethylene-co-TBA)

In a Schlenk flask, the catalyst (25 mg, 41.5 μmol) and TBA (50 ml, 0.35 mol) were dissolved in 100 ml of toluene under stirring. This solution was then introduced into a stainless steel reactor stirred by a baffle (800 rpm). It was immediately pressurized with ethylene (7 atm), and heated to 100 ^{o}C. After 2 hours at 100 ^{o}C, the reactor was cooled to room temperature and slowly depressurized. The polymer was precipitated in methanol (800 mL) and was washed 5 times with methanol. It was then filtered and dried under vacuum at 60 ^{o}C overnight. The acrylate incorporation was determined by ^{1}H NMR and conductimetric titration (*vide infra*). Copolymers of various levels of acrylate incorporation were obtained by adjusting the amount of acrylate and the ethylene pressure.

^{1}H NMR (600 MHz, T = 120 ^{o}C, TCE-d_2, δ): 2.1 (m, 1H, C**H**$CO_2{}^{t}$Bu), 1.4 (m, 2H, C**H$_a$**H$_a$'$CHCO_2{}^{t}$Bu C**H$_a$**H$_a$'), 1.3 (m, 9H; C$(CH_3)_3$) 1.2-0.9 (m, C**H$_2$**); ^{13}C NMR (121 MHz, T = 120 ^{o}C, TCE-d_2, δ): 176.0 (C=O), 79.8 (**C**$(CH_3)_3$), 46.7 (**C**HCO_2tBu), 32.8 (**C**H_2CHCO_2tBu), 29.8 (**C**H_2), 28.3 (C(**C**$H_3)_3$), 27.5 (**C**H_2CH_2CHCO_2tBu); IR (ATR): *v* = 2918.9 (m), 2849.7 (m), 1730 (s), 1473 (s), 1366 (m) 1151 (w).

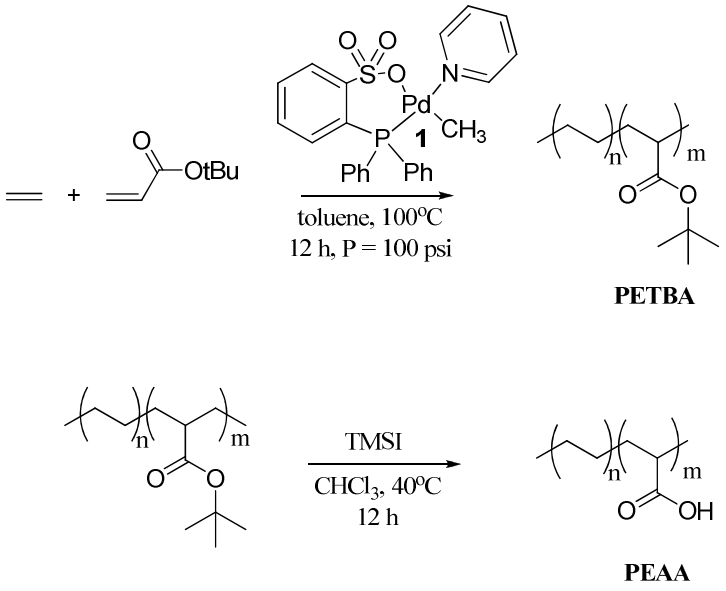

Scheme 2.1. Preparation of the polymers

2.3.3 Molecular weights determination

Molecular weights were determined by gel permeation chromatography (GPC) using a Viscotek HT GPC equipped with triple detection (RI, light scattering and viscometer) operating at 160°C. The eluent was 1,2,4-trichlorobenzene, and separation was performed on three PolymerLabs Mixed B(-LS) columns. The dn/dc of pure linear polyethylene was found to be 0.106 mL/g at this temperature. The dn/dc of several copolymers was also determined. A linear extrapolation between the dn/dc of the copolymers and the %weight composition in TBA was then performed, leading to the determination of an extrapolated dn/dc value of pure poly(*tert*-butyl acrylate) (0.0565 mL/g) under these conditions. The dn/dc of any copolymer was then calculated as the weighted-average of the dn/dc of pure PE and dn/dc of pure poly(*tert*-butyl acrylate).

2.3.4 Preparation of poly(ethylene-co-AA)

Trimethylsilyl iodide (TMSI, 0.12 mL, 0.840 mmol) was added to a solution of PETBA12 (259 mg) in chloroform (30 mL) placed in a 100-mL three-neck flask equipped with a condenser and a nitrogen inlet and immersed in an oil bath (~40 ^{o}C). The mixture was stirred at 40 ^{o}C under N_2-atmosphere overnight. A few drops of a solution of THF/water (8:2 v/v) were added to quench the reaction, followed by ~ 5 mL of a saturated sodium thiosulfate aqueous solution, yielding a pale yellow solution. The solvent was removed in a rotary evaporator. The recovered solid was dispersed into THF (50 mL). The suspension was stirred for 1 h and subjected to centrifugation (2250 rpm, 40 min). The supernatant was recovered and subjected to further purification by centrifugation (at least twice) until it was clear. It was concentrated under vacuum to ~ 3 mL. This solution was added dropwise to aqueous HCl (200 mL, 1.0 N). The precipitated PEAA12 was separated by filtration and dried in vacuum for 24 h. Yield: 65% (155.0 mg, 12 mol% of acrylic acid). Copolymers of other compositions were prepared via the same procedure applied to the other PETBA samples. ^{1}H NMR (600 MHz, THF-d_8, δ): 2.4 (m, 1H, COOH) 2.10 (m, 1H, C**H**COOH), 1.46 (m, 2H, C**H$_a$**H$_a$'CH(CO$_2$H)C**H$_a$**H$_a$'), 1.31 (m, 2H, CH$_a$**H$_a$'**CH(CO$_2$H)CH$_a$**H$_a$'**) 1.2 (m, C**H$_2$**); ^{13}C NMR (150 MHz, THF-d_8, δ): 177.3 (C=O), 46.2 (CH) 33.4 (**C**H$_2$CH(COOH)) 30.6 (CH$_2$) 28.4 (**C**H$_2$CH$_2$CH(COOH)) IR (ATR): ν = 2915 (s), 2848 (s), 1704 (m), 1471 (m), 730 (m), 718 (m).

2.3.5 Conductimetric titrations

An aqueous solution of sodium hydroxide (10 mL, 0.02N) was added dropwise to a solution of poly(ethylene-co-acrylic acid) (40.9 mg, 12 mol% AA) in THF (5 mL). An aqueous solution of HCl (0.02N) was added dropwise to the mixture and the changes of pH and conductivity upon addition were monitored, respectively, with a pH-meter (Corning pH meter 430 (95-98% slope)) and a conductivity meter (VWR Digital Conductivity Meter micromho) until the pH reached a value of 2. During this back-titration, the conductivity decreased rapidly until excess NaOH was neutralized, it increased slightly after the point of neutralization of all carboxylates. Further addition of HCl resulted in a sharp increase of the solution conductivity. The amount of HCl added within the nearly flat part of the titration curve was used to calculate the number of moles of COOH linked to the copolymer (see *Figure 2.7-S9*, Supporting Information).

2.3.6 Preparation of colloidal solutions of PEAA12

An aqueous NaOH solution (0.02 N, 15 mL) was added dropwise over 10 min to a stirred solution of PEAA12 (25 mg, 12 mol% AA) in THF (10 mL) yielding a turbid mixture that was stirred for an additional 20 min at the end of the addition. The suspension was dialyzed (Millipore membrane, MWCO 1000) against water until the pH of the dialysate reached a constant value (~ 7.0). The final colloidal solution (25 mL, c = 1 g/L) was opalescent.

2.3.7 Dynamic light scattering measurements (DLS)

DLS measurements were performed with an ALV/LSE-5003 DLS equipped with a Multiple Tau Analyzer Correlator, a He-Ne laser (λ = 633 nm), and a C25P circulating

water bath (Thermo Haake). The autocorrelation function was fitted for times ranging from 8 μs to 10 ms (102 datapoints) using the DLS-exponential $g_2(t)$ fitting routine. Samples for analysis (1.0 g/L) were filtered through 0.45 μm PVDF filters prior to measurement. They were kept in the sample cell for 20 min prior to analysis in order to ensure temperature equilibration. A cumulant analysis was applied to obtain the diffusion coefficient (D) of the scattering objects in solution. Their hydrodynamic radius (R_h) was obtained using the equation:

$$D = \frac{k_B T}{6\pi\eta_s R_h} \tag{2.1}$$

where k_B is the Boltzmann constant, η_s is the viscosity of the solvent (water) and T is the absolute temperature.

2.3.8 High-Sensitivity Differential Scanning Calorimetry (HS-DSC)

HS-DSC measurements were performed on a VP-DSC microcalorimeter (MicroCal Inc.) at an external pressure of ca. 180 kPa. The cell volume was 0.517 mL. The heating and cooling rate was 1^{o}C/min. Suspensions for analysis (copolymer concentration: 1 g/L) were prepared as stated above. Concentration of the copolymer was calculated by dividing the mass of the polymer by the total volume after dialysis. The suspensions were then filtered on 0.45 um PVDF filter and degassed at 25^{o}C for 20 min. By comparing the integral of the melting endotherm of a filtered sample to unfiltered one, it was concluded that filtration resulted in a 14% mass loss; therefore, the polymer concentration after filtration was 0.86 g/L.

Once introduced in the instrument, the colloidal solutions were equilibrated at 10 ^{o}C for 10 minutes before initiation of the heating process. For each measurement, the

sample was heated from 10 to 80 ^{o}C, maintained at 80 ^{o}C for 2 minutes and cooled to 10 ^{o}C. This heating and cooling treatment was repeated three times. The results presented are for the second or third heating scans, which, for a given sample, were identical within experimental precision. Data were corrected for instrument response time to take into account the effect of scan rate on the data collected. For each solution, the excess heat capacity curve was constructed by subtraction of water vs water scan from the sample vs water scan.

2.3.9 Transmission Electron Microscopy

The observations were performed on a FEI Tecnai 12 microscope at an accelerating voltage of 120 kV, equipped with a Gatan 1MPixel digital camera and a field emission gun. A phosphotungstic acid aqueous solution (70 μL, c = 1 wt%) was added to the colloidal solution (10 mL copolymer concentration ranging from 0.1 g/L to 0.01 g/L) as negative staining agent. The solutions were filtered through a 0.45 μm PVDF filter. A drop of the solution was placed on a Cu grid coated with formvar. The grid was dried in air overnight prior to imaging.

2.3.10 X-ray Diffraction measurements

XRD pattern were obtained with a Bruker diffractometer (D8 Discover), equipped with a Hi-Star area detector and using Cu K_{α} radiation (λ=1.542 Å, graphite monochromator). The X-ray tube was operated at 40 kV and 40 mA. The diffraction pattern was recorded with a Bruker AXS two-dimensional wire-grid detector. Solid polymer samples were analyzed directly after synthesis, without any heat treatment. The samples were packed into capillary tubes 1.0 mm in diameter (Charles Supper). Using GADDS 4.1.14 software, 1-D data were obtained integrating the 2-D data. The d-

spacings were determined using the Eva analysis software, and the Debye-Scherrer lengths were obtained by fitting each peak by a Gaussian.

2.4 Results and Discussion

2.4.1 Preparation and characterization of poly(ethylene-co-acrylic acid) samples

The copolymers were prepared by catalytic copolymerization of C_2H_4 with TBA and deprotection of the *tert*-butyl ester to afford PEAA (Scheme 1). The copolymerization of TBA with C_2H_4 was conducted using catalyst **1** (Scheme 1) developed previously for the copolymerization of ethylene with methyl acrylate.[28-30,34] The level of TBA incorporation was determined by ^{1}H NMR spectroscopy, by comparing the integral of the methine proton resonance CH(COO^{t}Bu) to all other resonances (*Figure 2.7-S1-S3*, Supporting Information). The absence of acrylate dyads in the quantitative ^{13}C NMR spectra of the copolymers (*Figure 2.7-S3*, Supporting Information) was taken as evidence that each acrylate unit is separated from another one by one or more ethylene unit. By varying the monomers feed in the copolymerization (i.e. acrylate concentration or ethylene pressure), we obtained 7 linear copolymers of ethylene and TBA (PETBA) containing from 4 to 17 mol% acrylate (*Table 2.1*). For the sake of brevity, the notation PETBAx (resp PEAAx) will designate the copolymer incorporating x mol% of TBA (resp. AA).

For the second step, we set out to hydrolyze the TBA groups with anhydrous trifluoroacetic acid, a method frequently used to carry out polymer-analogous conversion of the *tert*-butyl ester group into carboxylic acid.[36] For solubility reasons, the reaction was carried out in an anhydrous mixture of dichlorobenzene and trifluoroacetic acid (80:20 v:v) at 90 ^{o}C. The reaction progress was monitored by following the disappearance of the ester carbonyl stretching band at 1730 cm^{-1} in the FTIR spectrum of

the mixture. The appearance of two bands, one at 1706 cm^{-1}, attributed to the stretching vibration of isolated carbonyls of COOH groups, the other one at 1743 cm^{-1}, attributed to H-bonded COOH dimers,[37] confirmed the success of the conversion (see *Figure 2.7-S7*, Supporting Information).

Monomer incorporation x[a], mol%	PETBAx				PEAAx		
	M_n[b], g/mol	PDI[b]	T_m (^oC)[c]	$\Delta H_{melting}$(J/g)[c]	T_m, (^oC)[c]	$\Delta H_{melting}$(J/g)[c]	COOH[d] mol%
4	7800	1.5	102	103	nd	nd	nd
7	5800	1.9	90	59	114	99	nd
10	3800	1.3	66	32	80	79	nd
12	3000	1.2	60	18	76	44	12.0
16	3000	1.2	42	9	62	12	15.9
17	2800	1.2	nd[e]	nd	nd	nd	17.1

[a] Determined by ^1H NMR analysis [b] Determined by GPC analysis at 160 °C in 1,2,4 trichlorobenzene. [c] Determined by DSC of the solid sample. [d] Determined by conductimetric titration. [e] Not determined

Table 2.1. Physical properties of the polymers.

Unfortunately, the polymers recovered *in their dry form* after purification resisted dissolution in any solvent. Their insolubility is attributed to the formation, in the absence of water, of an extensive H-bond network among carboxylic acid groups, as evidenced by the FTIR spectrum of the samples. These polymers were not used for further

manipulations. To circumvent this insolubility problem, we used a different method known to cleave esters into carboxylic acids under milder conditions [38-40]. The ester groups of PETBAx were converted into trimethylsilyl carboxylates by treatment with trimethylsilyl iodide. Subsequent aqueous hydrolysis led to PEAAx which were not involved in extensive H-bond networks, as shown by the samples FTIR spectra, which presented a band in the carbonyl stretching spectral region located at 1704 cm^{-1}, a wavenumber typical of the stretching of carbonyls of isolated COOH, together with a broad absorption in the 3000 cm^{-1} region due to the presence of H-bonds with traces of water (from the final hydrolysis step). The FTIR spectra presented only a minute absorption at 1743 cm^{-1} (see *Figure 2.7-S8*). This synthetic procedure led to polymers which could be redissolved either in THF at room temperature (COOH molar incorporation ≥12 mol%) or in tetrachloroethane at 120 ^{o}C (COOH molar incorporation ≤ 12%). However, it should be noted that complete dehydration (for example by heating a polymer above its melting point) resulted in a polymer which, in our hands, was insoluble, due to the formation of intermolecular H-bonds (as indicated by FTIR spectroscopy). Analysis of quantitative ^{1}H and ^{13}C NMR spectra, measured at room temperature for AA ≥ 12 mol% or at 120^{o}C for AA < 12 mol% (*Figures 2.7-S5-S6*, Supporting Information) confirmed that the copolymers were fully and cleanly deprotected. Thus, the ^{1}H NMR spectrum resonance at 1.95 ppm due to the methine protons C**H**(COO^{t}Bu) was replaced by a signal at 2.2 ppm attributed to the methine protons C**H**(COOH). In the case of copolymers containing 12 mol % AA and more, the molar incorporation of COOH was measured also by conductimetric titrations (see

Figure 2.7-S9) that yielded values in excellent agreement with data derived from quantitative NMR spectroscopy (*Table 2.1*).

2.4.2 Bulk properties of copolymers

Differential scanning calorimetry (DSC) measurements were carried out on copolymer samples heated at a rate of 0.3 ^{o}C/min following a pretreatment from 140 ^{o}C to 20 ^{o}C at a cooling rate of 0.3 ^{o}C (*Figure 2.1, Table 2.1*). The DSC traces of PETBAx samples present a single endothermic peak, from which we extracted the enthalpy of melting (ΔH) and the melting temperature (T_m). The ΔH values decreased significantly with increasing TBA incorporation; for example, the ΔH of PETBA16 is more than 10 times smaller than that of PETBA4, and 20 times smaller than that of pure polyethylene prepared under the same conditions, indicating that PETBA16 is nearly totally amorphous. This is confirmed by the X-Ray Powder Diffraction (XRD) pattern of this sample (*Table 2.2*) for which the amorphous broad peak dominates all other reflections. It is customary to calculate crystallinity by normalizing the enthalpy of melting of a copolymer by the enthalpy of melting of 100% crystalline polyethylene (294 J/g) [41]. This calculation implicitly assumes that the crystallite is identical to that of pure polyethylene. We will see below that it is not the case with the samples described here, hence the PETBAx crystallinity values cannot be determined by this method.

The melting points (T_m) of the copolymers also decreased with increasing comonomer incorporation, and all values were lower than the T_m of PE, as shown in *Figure 2.1*, where we present a plot of the changes in T_m of PETBAx as a function of co-monomer content. We included on the plot the T_m values of copolymers of ethylene and other nonionic monomers, such as poly(ethylene-co-methylacrylate) and poly(ethylene-*co*-N-vinyl pyrrolidinone), which were prepared by catalytic copolymerization using the same catalyst (**1**, Scheme 1) as in the synthesis of the PETBAx samples.[30,32] The melting

points of all the copolymers fall on the same line, in agreement with the Flory exclusion model,[42] which stipulates that the substituents introduced by a co-monomer are excluded from the PE crystallite. Increasing co-monomer incorporation results in smaller crystallites and lower melting points, irrespective of the nature of the co-monomer.

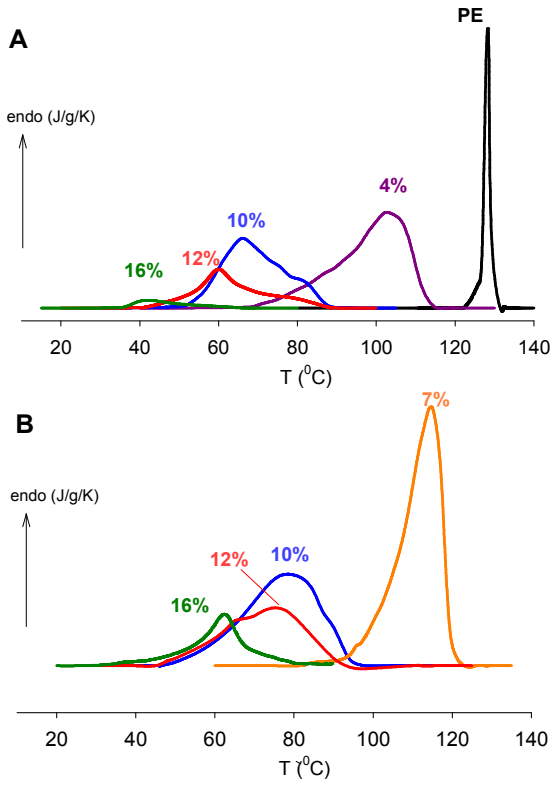

Figure 2.1. DSC melting endotherms of bulk PE and PETBAx (**A**) PEAA (**B**); the % values represent the level of comonomer (TBA or AA) incorporation in mol%.

The melting points of the PEAAx samples are also shown in *Figure 2.2.* They are systematically higher by ~ 10 ^{o}C, compared to their PETBAx precursors and deviate significantly from the Flory exclusion model line constructed using melting points of copolymers of ethylene and nonionic polar monomers (*Figure 2.2*). This observation necessarily implies that some of the COOH groups may in fact be included in the PE

crystal cell. Further support for this hypothesis was gathered by analysis of XRD data recorded for bulk copolymers. The diffraction pattern of each copolymer was resolved into two peaks, one at an angle $2\theta = 21.3 +/- 0.2^{o}$, corresponding to the 110 reflection, and the other one at $2\theta = 23.5 +/- 0.2^{o}$, corresponding to the 200 reflection, both for an orthorhombic unit cell (see Figure S10, Supporting Information).

Polymer	Angle 2Θ (°)	Debye-Scherrer particle size , nm	Lattice spacing, Å
PE[a]	21.6 [a] 24.0 [a]	nd	b = 4.93 [a] a = 7.40 [a]
PEAA4	21.4 23.8	24	b = 4.98 a = 7.46
PEAA7	21.4 23.7	22	b = 4.98 a = 7.50
PEAA10	21.35 23.5	17	b = 4.97 a = 7.58
PEAA12	21.25 23.3	15	b = 4.99 a= 7.62
PEAA14	21.2		
PEAA16	amorphous		
PEAA17	amorphous		

Table 2.2. X-ray diffraction data for samples of PE and PEAAx. For copolymers with AA incorporations larger than 14 mol%, the amorphous broad peak dominates and no separate reflection can be observed.

These reflections were used to calculate the dimensions of the copolymers unit cell that are listed in *Table 2.2*, together with the known dimensions of the unit cell of orthorhombic polyethylene (a = 7.40 Å and b = 4.93 Å).[42] For all copolymers, the *a* spacing is significantly larger than the *a* value of the polyethylene unit cell, while the *b* spacing is identical, or very close, to the *b* spacing of pure polyethylene (*Table 2.2*). This lattice expansion must be ascribed to the accommodation of some, but not necessarily all, COOH groups as crystalline defects in the PE crystals. This observation is in good agreement with existing data for 'precision' PEAA samples prepared by ADMET[17]. These defects are generally expected to weaken the crystal cell (lower melting point), but in our case, intracrystalline H-bonds due to adjacent COOH groups can reinforce the crystals and enhance their melting point.

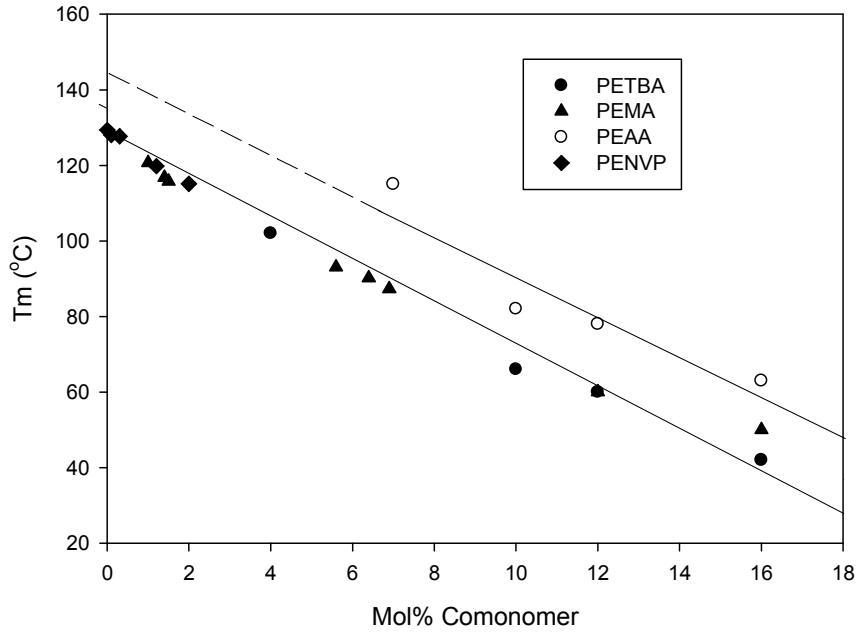

Figure 2.2. Changes of the melting point (T_m) of copolymers prepared by catalytic polymerization as a function of comonomer incorporation (in mol %). The melting points

of PEMA (poly (ethylene-co-methyl acrylate) and PENVP, poly(ethylene-co-N-vinylpyrrolidinone), are taken from reference 32. The lines are to guide the eye.

2.4.3 Amphiphilic properties of poly(ethylene-co-AA) and nanoparticle formation

Among the various copolymers prepared, only PEAA12 is both crystalline and readily soluble in organic solvent. Samples of lower AA content are crystalline, but only scarcely soluble at ambient temperature, while samples of higher AA content dissolve readily in organic solvents, but are not crystalline. Since one specific objective of this study was to assess the impact of crystallinity on the self-assembly of amphiphilic copolymers in water, we focused our attention to the properties of PEAA12 solution in THF with aqueous sodium hydroxide (0.02 N) following a protocol described in the experimental section. The resulting mixture was subjected to extensive dialysis against water to remove excess NaOH and THF. This procedure led to the formation of an opalescent fluid (pH = 7). The size and size distribution of the nanoparticles in suspension were determined by dynamic light scattering (DLS) measurements carried out with a fluid for which the copolymer concentration was adjusted to 1.0 gL^{-1}. The major population of objects in this fluid has an average hydrodynamic radius (R_h) around 12 nm. A minor population, representing less than 5% in weight, was detected in the larger size domain (R_h ~ 88 nm). Visualization by TEM of the air-dried fluid confirmed the presence of nanoparticles. The micrographs feature elongated objects, with an average polar radius of 49 nm (σ = 15.0 nm) and an equatorial radius of 9 nm (σ = 3.0 nm), together with a few occasional larger particles (*Figure 2.3 and Figure 2.7-S11*, Supporting Information). The discrepancy between the nanoparticles radii measured by DLS and TEM is to be expected when one recalls that the hydrodynamic radius of non-spherical particles is not equal to their geometrical radii. The hydrodynamic radius

obtained from DLS measurements derives, via the Stokes-Einstein equation, from the nanoparticle self-diffusion coefficient, which for an elongated particle of length L and cross-section d in water of viscosity η at a temperature T, can be expressed as:

$$D = \left(\frac{k_B T}{3\pi\eta L}\right)\left(\ln p + 0.312 + \frac{0.565}{p} - \frac{0.100}{p^2}\right) \qquad (2.2)$$

where p = L/d.[44,45] Using the values of L and d obtained by TEM, the calculated value of D is 2.09 × × 10^{-11} m^2s^{-1} at 25 ^oC. The Stokes-Einstein formula ($D = k_BT/6\pi\eta R_h$) can then be used to calculate a hydrodynamic radius R_h of 11.7 nm, a value which is in excellent agreement with the DLS measurement.

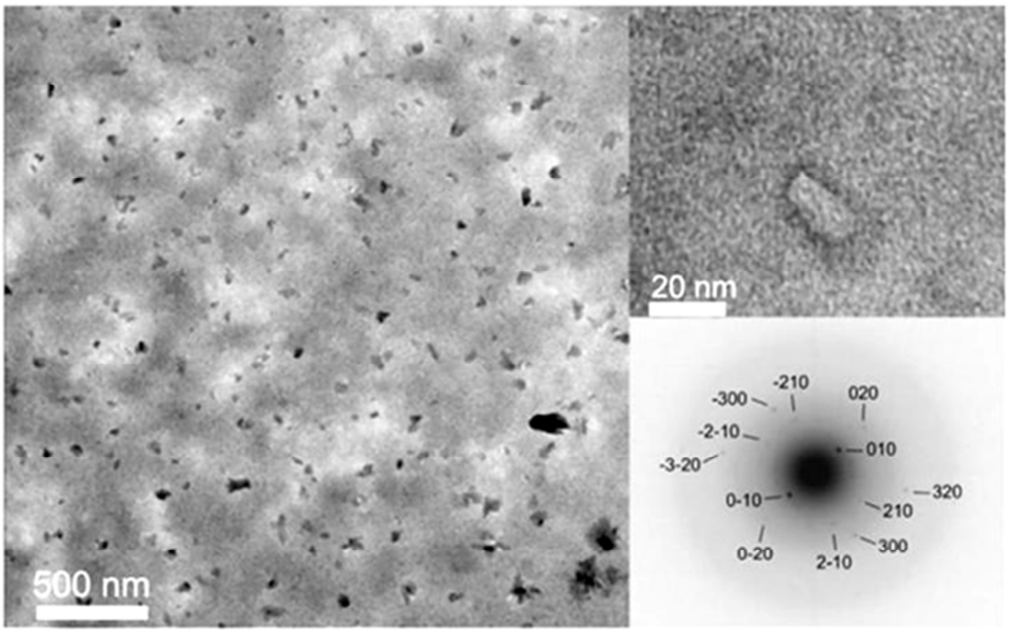

Figure 2.3. TEM micrographs of nanoparticles obtained from dialyzed suspensions of PEAA12 (upper right: enlarged view of one of the particles; lower right: electron diffraction pattern obtained for one nanoparticle).

The morphology of the rod-like particles is reminiscent of the shape of the surfactant-stabilized nanoplatelets of pure crystalline PE obtained by catalytic emulsion polymerization of ethylene in water[25]. It suggests that the colloidal PEAA12 nanoparticles contain crystalline domains. Analysis of single nanoparticles by High-Resolution Transmission Electron Microscopy (HR-TEM) yielded electron-diffraction patterns (*Figure 2.3*) consistent with the orthorhombic lattice of a PE monocrystal (a = 7.37 Å and b = 4.93 Å)[45]. This demonstrates that each nanoparticle, which was colloidally stable in water, contains in fact one isolated monocrystal. However, the point to point resolution of the pattern is not ascertain whether the monocrystal lattice if that of pure PE or that of a slightly dilated PE cell in which COOH groups are present.

2.4.4 Temperature-responsiveness of aqueous colloidal poly(ethylene-co-AA) fluids

A high-sensitivity DSC scan recorded upon heating a colloidal suspension of PEAA12 (c = 1.0 g/L) at a rate of 1.0 ^{o}C per min is presented in *Figure 2.4*, together with the scan recorded upon cooling the sample at the same rate. The trace corresponding to sample heating presents an endotherm with a maximum (T_m^{coll}) at 62 ^{o}C and an enthalpy of 81 J/g. Upon cooling, an exotherm is observed at a temperature of 48 ^{o}C, which is 14^{o}C lower than the transition taking place upon heating. Rescanning the sample under identical conditions leads to identical thermograms. Turning our attention first to the heating scan, we note that the T_m^{coll} is nearly identical to the melting temperature of bulk PETBA12 bulk (60 ^{o}C, see *Figure 2.1* and *Table 2.2*). This similarity suggests that the endothermal transition observed when heating the nanoparticles in water corresponds in fact to the melting of the crystals within the nanoparticles. This hypothesis is strengthened by two additional facts: (i) the difference between temperature maxima recorded upon heating and subsequent cooling is reminiscent of the supercooling effect expected for a polymer crystallization process. A supercooling effect of 70 ^{o}C has been reported recently for the melting/crystallization of polyethylene nanoparticles[25, 47]; (ii) the T_m^{coll} value is different from the T_m of bulk PEAA12 (76 ^{o}C, see *Figure 2.1A* and *Table 2.2*), but corresponds to the melting point of bulk PETBA (see above). This observation implies that the endotherm observed reflects the melting of crystalline PE, as in the case of PETBA12 (see above), rather than the melting of a crystal that incorporates COOH defects within its lattice, as in the case of bulk PEAA12. The enthalpy of the transition of the aqueous colloidal PEAA12 dispersion does not correspond to the enthalpy of bulk

PETBA12. It is significantly larger (81 J/g vs. ~ 44 J/g for PEAA12 and 18 J/g for PETBA12 from *Figure 2.2*). Thus, the melting of the PE crystalline phase of suspended nanoparticles must be accompanied by additional endothermal effects that accompany changes in the interactions of the nanoparticles with its aqueous environment. From the HS-DSC results and the electron diffraction patterns, which prove that the nanoparticles contain a single monocrystal and an amorphous phase, we speculate that in the aqueous environment the energy gained during crystallization ($-\Delta H_{melting}$) is not sufficient to offset the heat of solvation of the partially deprotonated COOH (at pH=7, with Na^+ or H^+ counterions) forcing most polar substituents to stay in the amorphous phase when the crystal is formed. Furthermore, the presence of hydrophilic groups on the particles surface accounts for their colloidal stability of aqueous PEAA12 suspensions.

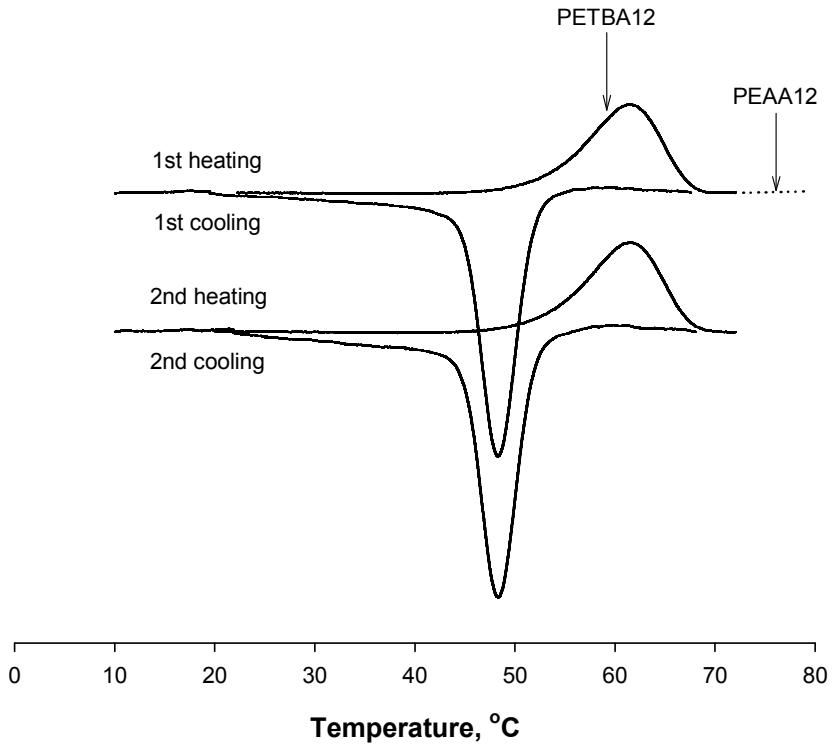

Figure 2.4. Thermograms of an aqueous dispersion of PEAA12 in water (~1 g/L) recorded by HS-DSC upon heating and subsequent cooling (heating/cooling rate: 1 ^{o}C/min). The arrows indicate the melting points of solid PETBA12 and PEAA12.

To probe the fate of the nanoparticles upon heating, we performed DLS measurements on aqueous colloidal PEAA12 suspensions heated to several temperatures between 20 and 65 ^{o}C. Representative size distributions are presented in *Figure 2.5*. At 20 ^{o}C, the suspension contains mainly particles of R_h = 12 nm as noted above. No significant changes are observed upon heating up to 55 ^{o}C.

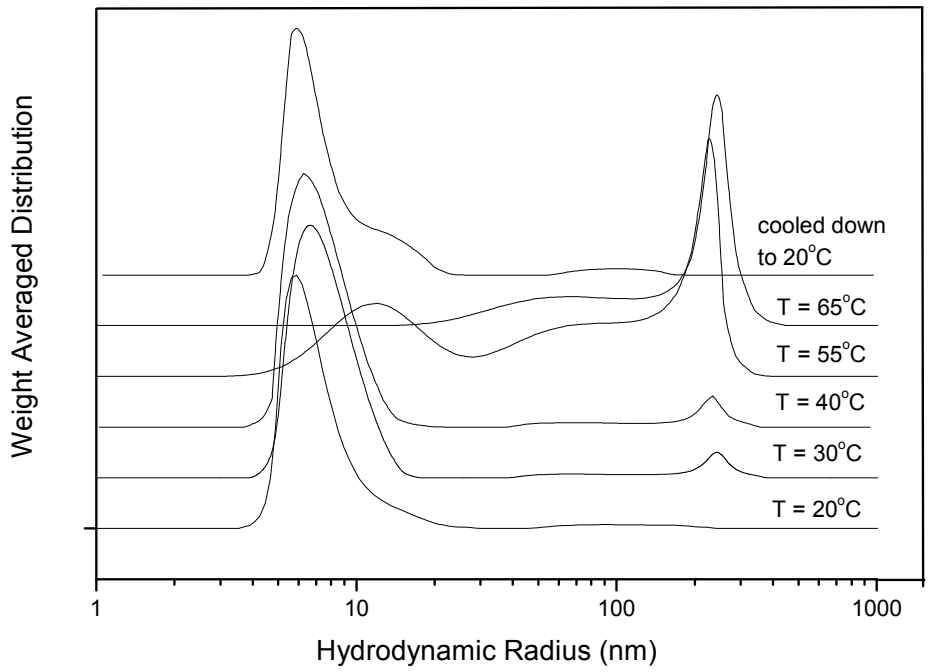

Figure 2.5. Hydrodynamic radii distributions recorded by DLS for a suspension of PEAA12 in water heated to various temperatures from 20 ^{o}C to 65 ^{o}C. The top trace corresponds to a sample cooled from 65 ^{o}C to 25 ^{o}C.

Above this temperature, the scattering profile has a significant contribution from particles of Rh ~ 240 nm, which become the major contributors in suspensions heated to 65 ^{o}C, i.e. above the melting temperature of PE. Hence, the originally crystalline nanoparticles coalesce into larger "nanodroplets", which remain colloidally stable in hot water and do not undergo macroscopic phase separation. The term "droplet" is an apt description of the particles, since the PE is in its liquid state at this temperature. Assuming that a droplet as an elementary nanoparticle has approximately the same density, we estimate that a droplet is constituted of about 180 elementary nanoparticles.

The coalescence of nanoparticles is believed to be triggered by the conservation of the interfacial energy upon melting of the PE crystal and reorganization of the interfacial structure associated with the enthalpy detected by HS-DSC measurements.

The topmost size distribution presented in *Figure 2.5* corresponds to a sample cooled from 65 ^{o}C to 25 ^{o}C and kept at this temperature for several hours. Remarkably, it is identical to the size distribution of the suspension prior to heating. The heating/cooling cycle was repeated three times without any changes in particle size distributions of either the cold or hot suspensions. Thus upon reaching the PE crystallization temperature, the droplet crystallizes and fragments to form crystalline nanoparticles of dimensions which are identical to the starting ones.

2.5 Conclusions

This work demonstrates that the most common polyolefin, namely polyethylene, can form well-defined surfactant free nanoparticles that are colloidally stable in water. In order for polyethylene to be dispersible in water, pendant COOH groups were introduced along the linear chain. The resulting polymer, linear PEAA, crystallizes in the bulk in the usual orthorhombic polyethylene unit cell where one of the cell dimensions is elongated in order to accommodate COOH groups as defects in the crystal.[42] The presence of H-bonded COOH groups within the crystal results in an increase of the melting point of the copolymer, in comparison to the melting point predicted by the Flory exclusion model. Using a solvent exchange procedure, followed by a dialysis, we were able to trigger the self-assembly of a PEAA copolymer with 12 mol% AA into nanoparticles freely suspended in water. Using a combination of electron diffraction and HS-DSC studies, we established that these particles are in fact constituted of a core of pure polyethylene

surrounded by a hydrated layer containing the COOH groups. Thus, the nanoparticles and the bulk polymer can be seen as two allomorphic forms of the same polymer. The crystallization into one or the other allotrope is directed by the presence (or absence) of water. Although well documented for small molecules, this behavior is rather uncommon for macromolecules. Heating a suspension past the nanoparticles melting temperature, triggers the coalescence of melted nanoparticles into nanodroplets of finite dimensions. This behavior is reversible: cooling the suspension below the copolymer melting point triggers the formation of colloidally stable crystalline nanoparticles similar in size to the nanoparticles prior to the heating/cooling treatment. Hence, the polyethylene nanoparticles are thermoresponsive. This intriguing and novel thermoresponsive behavior of ethylene copolymers opens the way to interesting applications as, e.g., for the generation of stimuli responsive nanomaterials for biomedical or environmental uses.

2.6 Acknowledgment

Financial support for this work was provided by the Fonds Québécois de la Recherché sur la Nature et les Technologies. FMW thanks Prof. T. Sato (Osaka University, Toyonaka, Osaka, Japan) for useful comments and suggestions on the work.

2.7 Supplementary Information

This part contains supplementary experimental results for the article.

2.7.1 Experimental Results

Table 2.7-S1. Synthesis conditions and main characteristics of poly(ethylene-co-*tert*butyl acrylate) copolymers

React. conditions					**Results**				**Polymer properties**				
Entry	Time hrs	Conc. cat. µmol/l	Conc tBA, mol/l	P_E atm	incorp x[a], mol%	yield g	TON[b] E	TON[b] TBA	M_n[c] g/mol	PDI[c]	Ave. F_w[d]	DP[e]	DP TBA[f]
1	1.5	89.6	0.69	7	4	1.8	3000	136	7800	1.5	32.4	240.7	9.6
2	1.5	88.7	0.34	20	7	0.98	1476	108	5000	1.9	34.9	143.3	10.0
3	2	89.1	1.7	7	10	0.43	568	64	3500	1.3	38.2	91.6	9,2
4	1.5	183	0.86	7	12	0.32	194	26	3000	1.2	39.8	75.4	9.0
5	15	183	0.86	7	16	0.30	154	30	3000	1.2	44.4	67.6	10.8
6	3	189	1.7	7	17	0.06	30	6	2800	1.2	48.2	58.1	9.9

[a] Determined by ^{1}H NMR analysis at 120 ^{o}C in 1,1,2,2 tetrachloroethane

[b] Turnover number = mole of substrate converted per mole catalyst

[c] Determined by GPC analysis at 160 °C in 1,2,4 trichlorobenzene

[d] Average molecular weight, calculated from TBA incorporation

[e] Degree of polymerization calculated from both M_n values and Ave. F_w

[f] Number of TBA units in the polymer chain, calculated from DP and the molar incorporation, x.

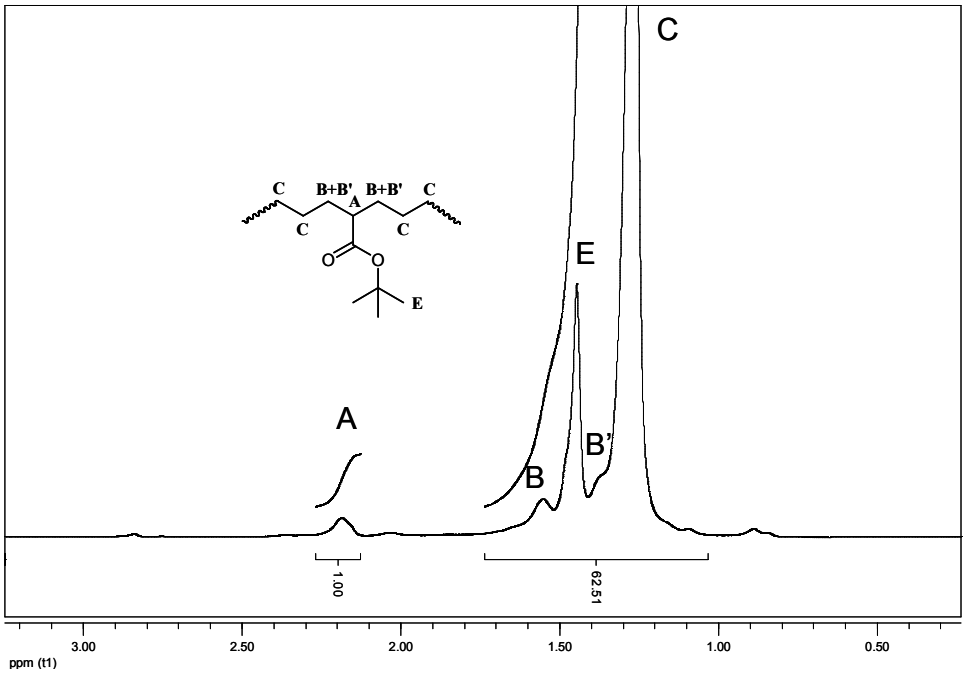

Figure 2.7-S1a. ^{1}H NMR of poly(ethylene-co-TBA) with 7 mol% of TBA. ($C_2D_2Cl_4$, T = 120 ^{o}C).

Calculation of the molar incorporation of TBA, x

I_A: integral of methine proton A - I_{chain}: integral of protons B, B', D and E

$$x = \frac{4I_A}{I_{rest} - 7I_A}$$

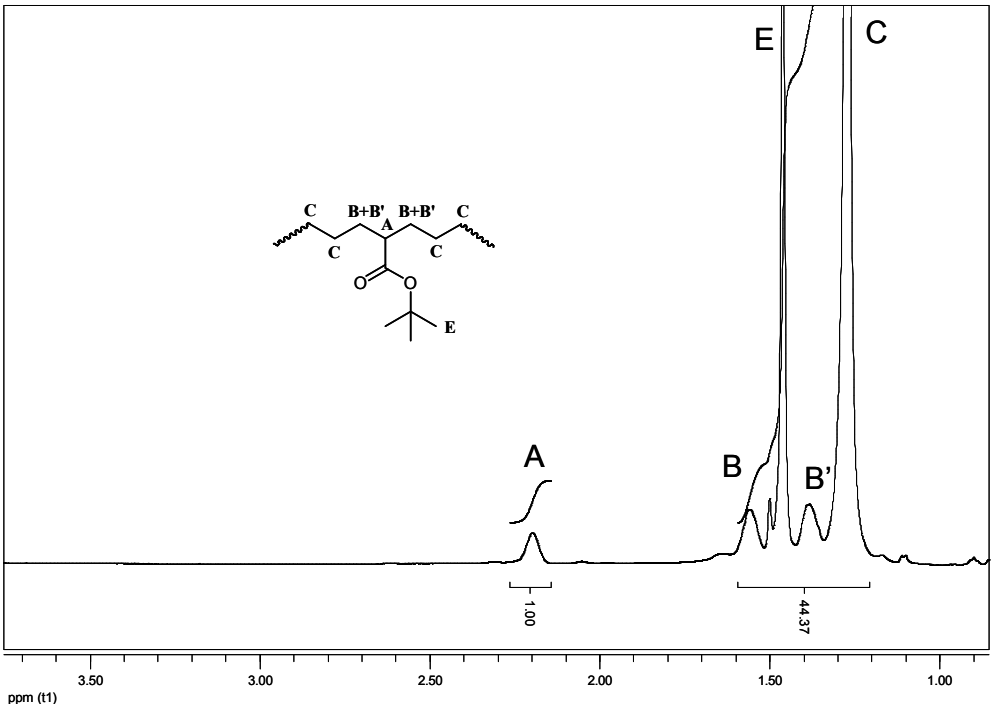

Figure 2.7-S1b. ^{1}H NMR of poly(ethylene-co-TBA) with 10 mol% of TBA. ($C_2D_2Cl_4$, T=120^{o}C).

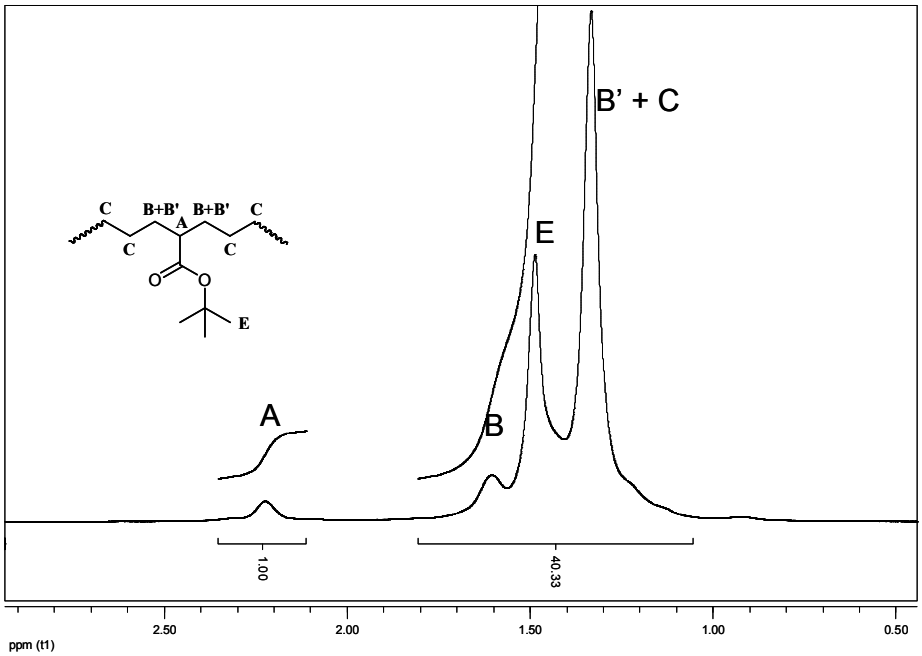

Figure 2.7-S1c. ^{1}H NMR of poly(ethylene-co-TBA) with 12 mol% of TBA. ($C_2D_2Cl_4$, T=120^{o}C).

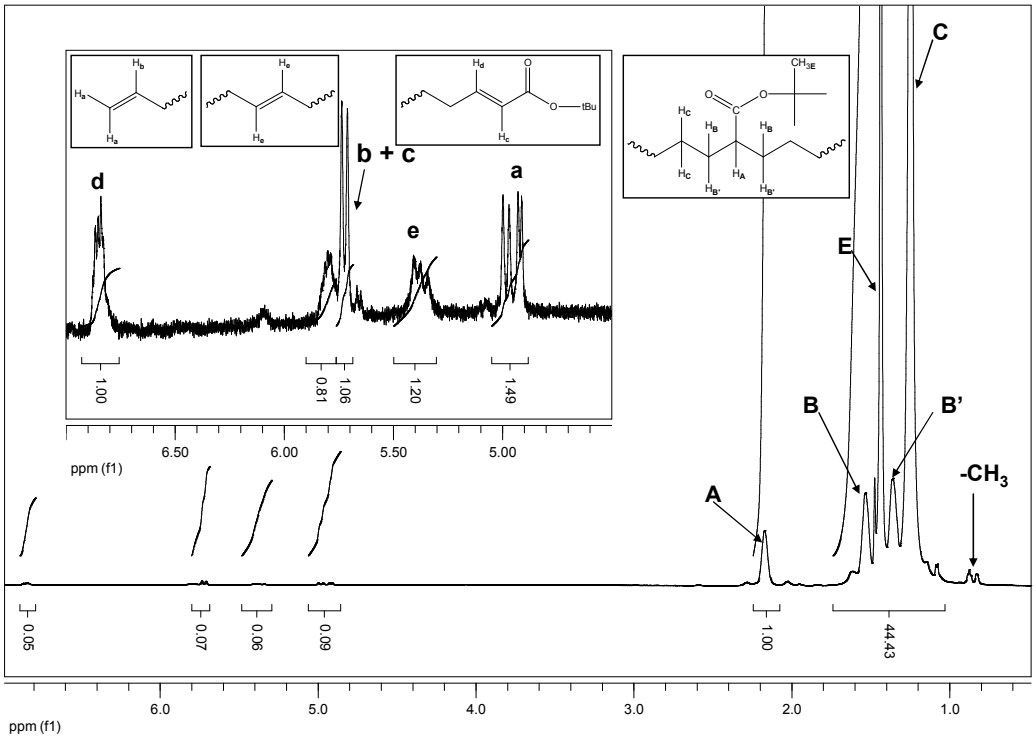

Figure 2.7-S2. ^{1}H NMR of poly(ethylene-co-TBA) with 10 mol% of TBA. ($C_2D_2Cl_4$, T = 120 ^{o}C). Insert: vinylic end-groups. The resonance labeled *e* corresponds to internal double bonds generated upon isomerization of terminal double bonds. Such isomerization is well established for palladium aryl sulfonate catalysts: see for example comment about octene insertion.

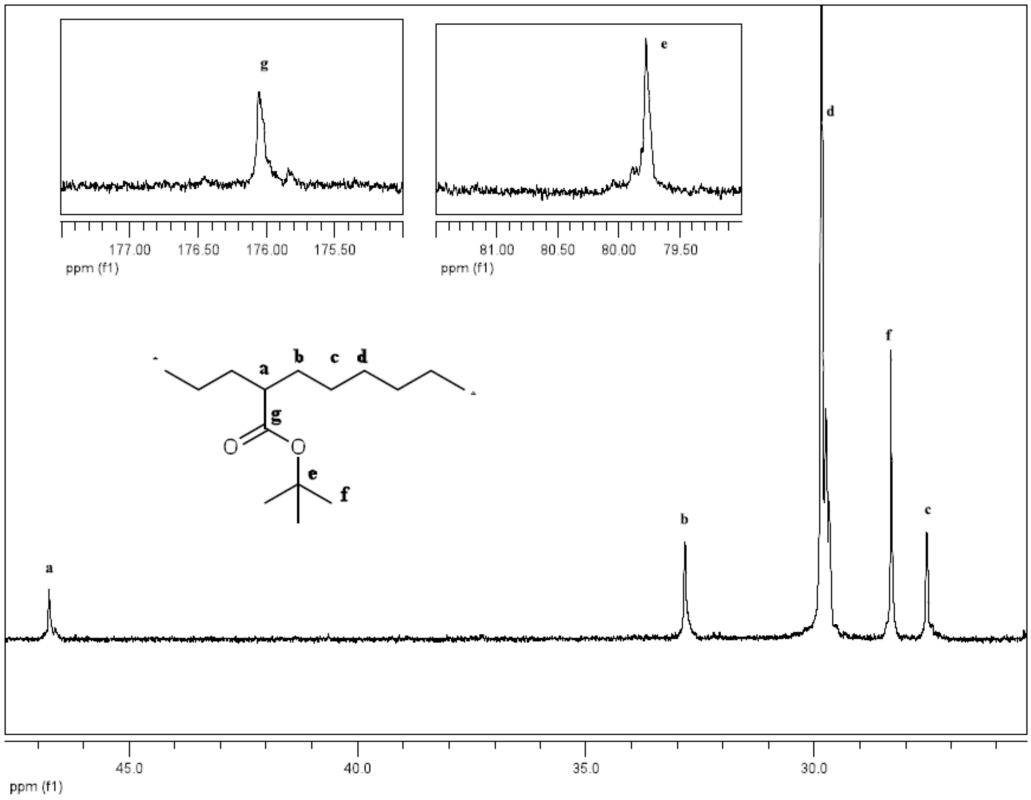

Figure 2.7-S3. ^{13}C NMR (quantitative) of poly(ethylene-co-TBA) with 12 mol% of TBA. ($C_2D_2Cl_4$, T = 120 ^oC). Using the data of on the insertion polymerization of methyl acrylate and ethylene, three types of resonances are possible for **C**H($CO_2{}^tBu$): one for consecutive acrylate dyads AA at 42 ppm, one for alternated acrylate triads AEA at 44 ppm, and one for isolated acrylate units at 46 ppm. The *a* resonance is therefore indicative of isolated acrylate units, in agreement with a copolymer with a random distribution.

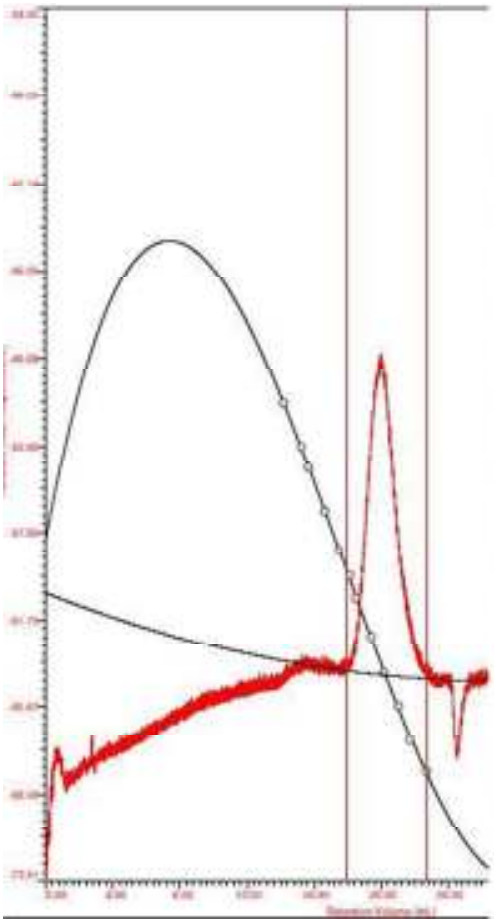

Peak RV - (ml)	19.987
Mn - (Daltons)	5,859
Mw - (Daltons)	8,869
Mz - (Daltons)	12,243
Mp - (Daltons)	7,822
Mw / Mn	1.514
Percent Above Mw: 0	0.000
Percent Below Mw: 0	0.000
Mw 10.0% Low	2,311
Mw 10.0% High	20,893
IV - (dl/g)	0.2422
Rh - (nm)	3.121
Wt Fr (Peak)	1.000
Mark-Houwink a	0.158
Mark-Houwink logK	-1.693
Branches	0.000
Branch Freq.	0.000
RI Area - (mvml)	27.69
UV Area - (mvml)	0.00
RALS Area - (mvml)	0.00
LALS Area - (mvml)	0.00
IVDP Area - (mvml)	47.92

Figure 2.7-S4. GPC trace of poly(ethylene-co-TBA) with 7 mol% of TBA. (ODCB, T = 160 ^{o}C). Flow rate: 1 ml/min. Columns (2): Mixed C-LS Polymer Laboratories. Detectors: RI, viscometer and light scattering. Calibration: triple detection.

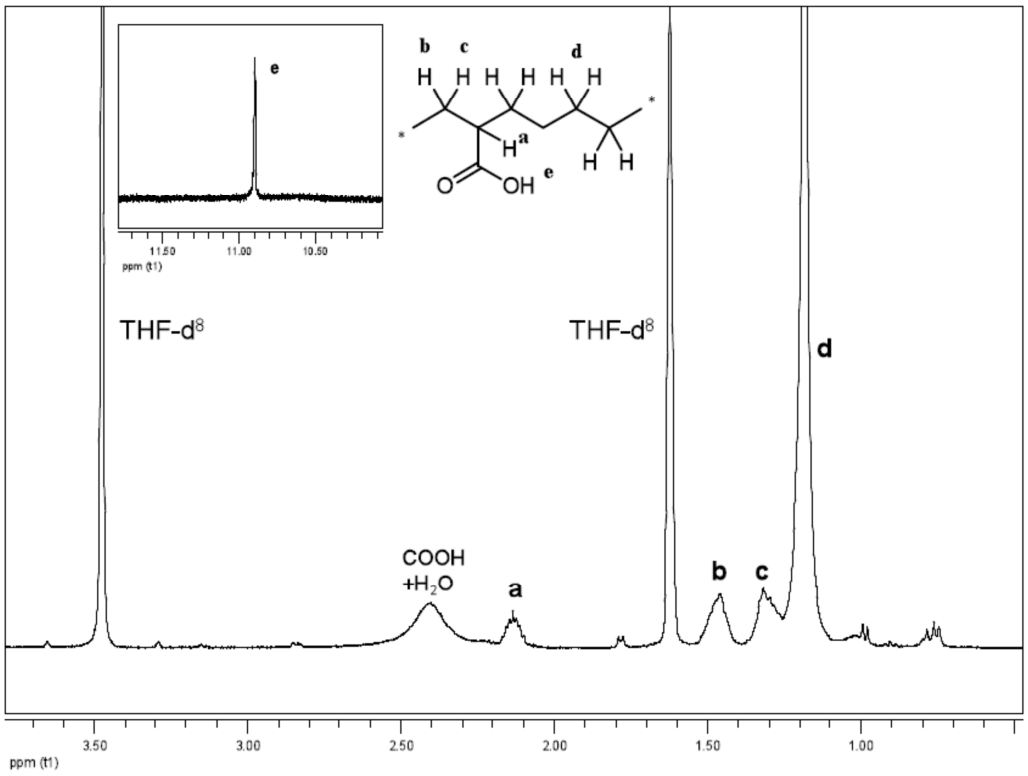

Figure 2.7-S5. ^{1}H NMR of poly(ethylene-co-AA) with 12 mol% of acrylic acid incorporation (THF-d^{8}).

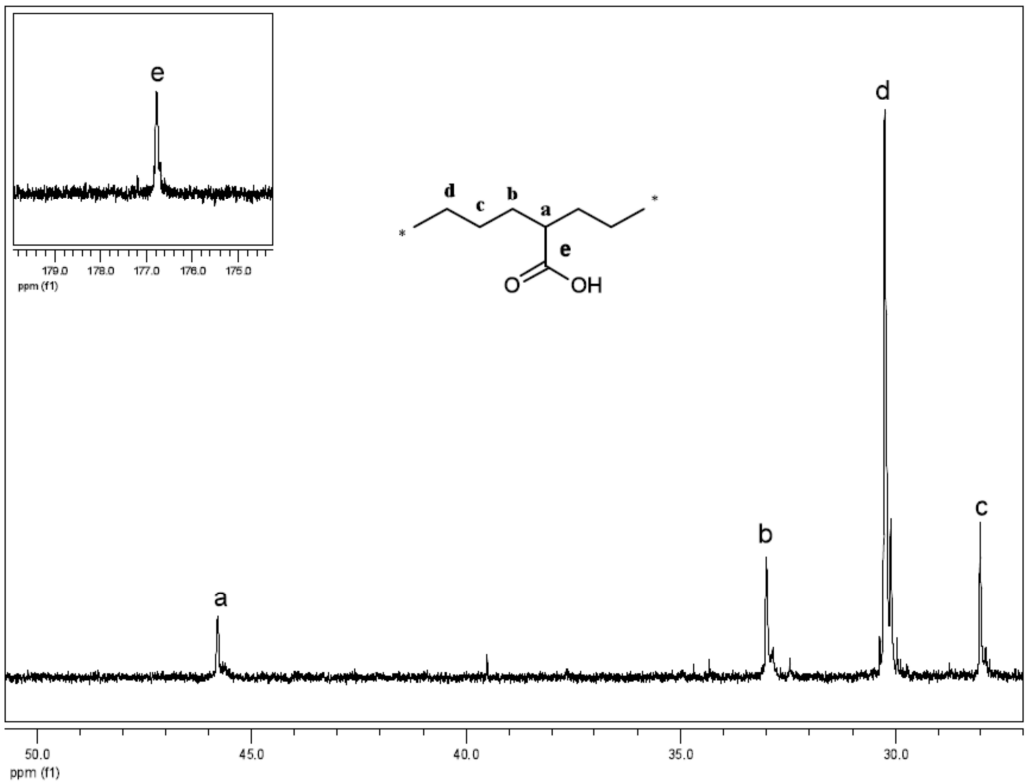

Figure 2.7-S6. ^{13}C NMR of poly(ethylene-co-AA) with 12 mol% incorporation of acrylic acid (THF-d^8).

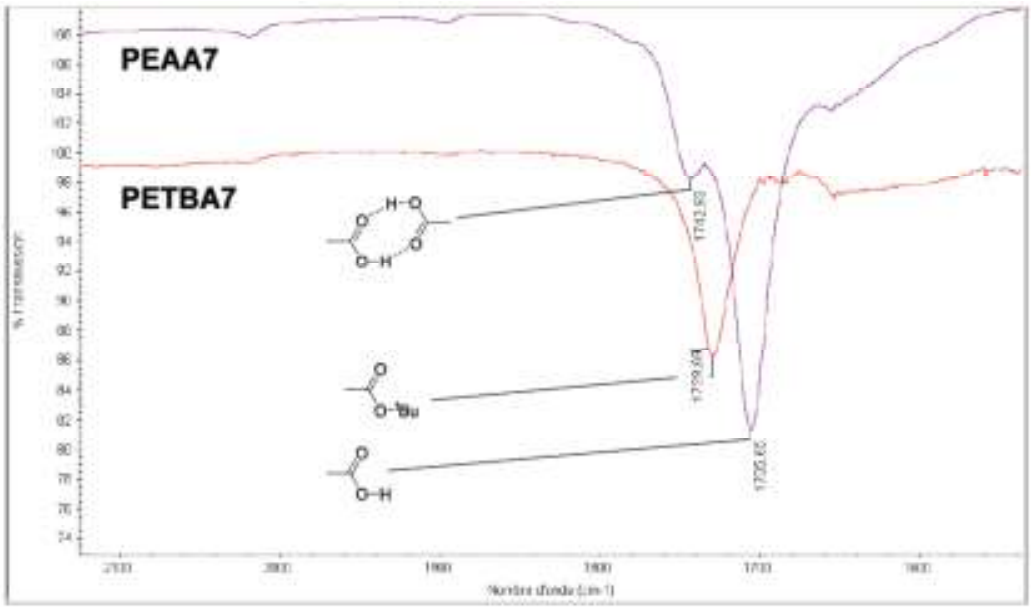

Figure 2.7-S7. FTIR of the polymers before and after treatment with TFA (C=O stretching region).

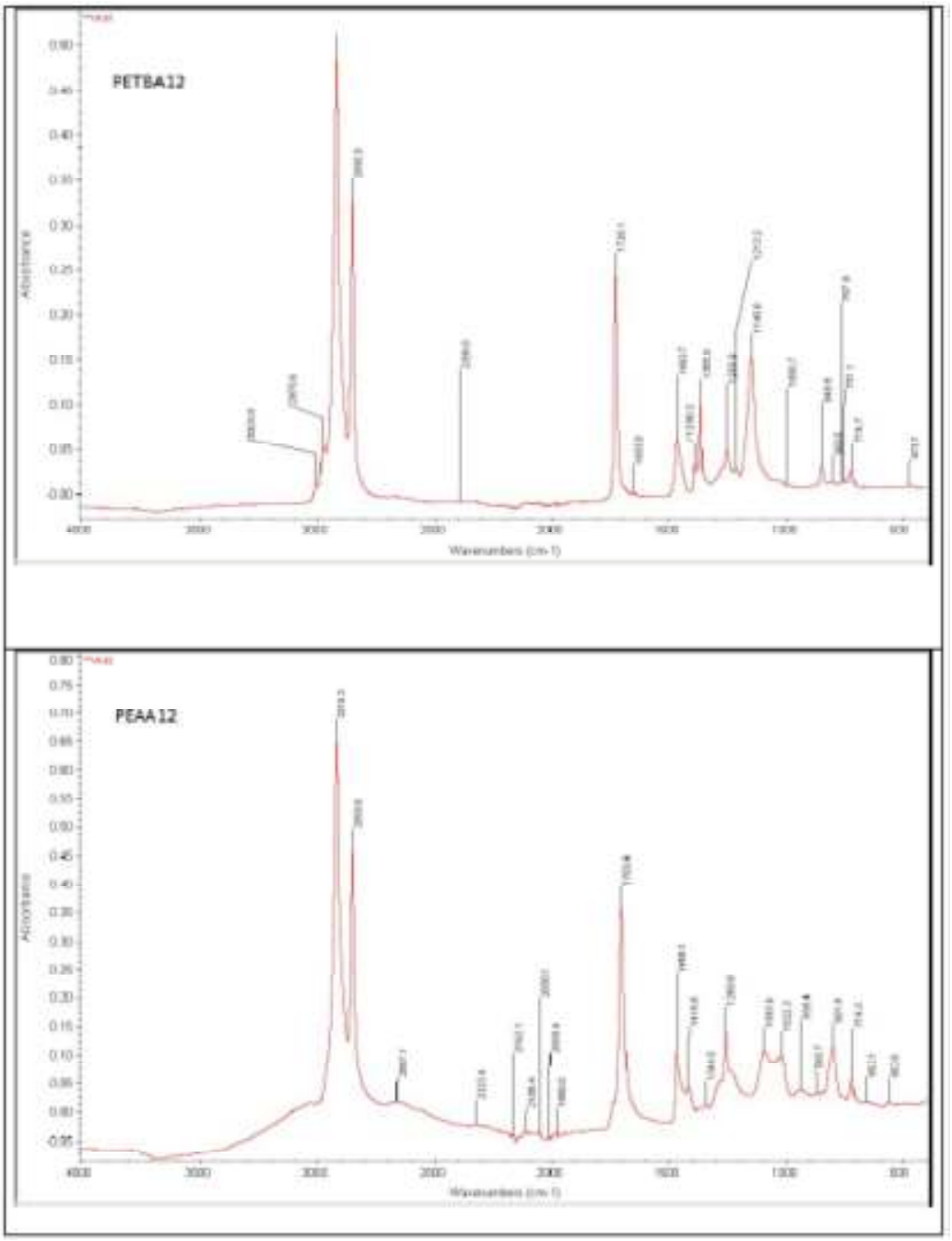

Figure 2.7-S8. FTIR of the polymers before (top) and after ester hydrolysis (bottom, using TMSI activation).

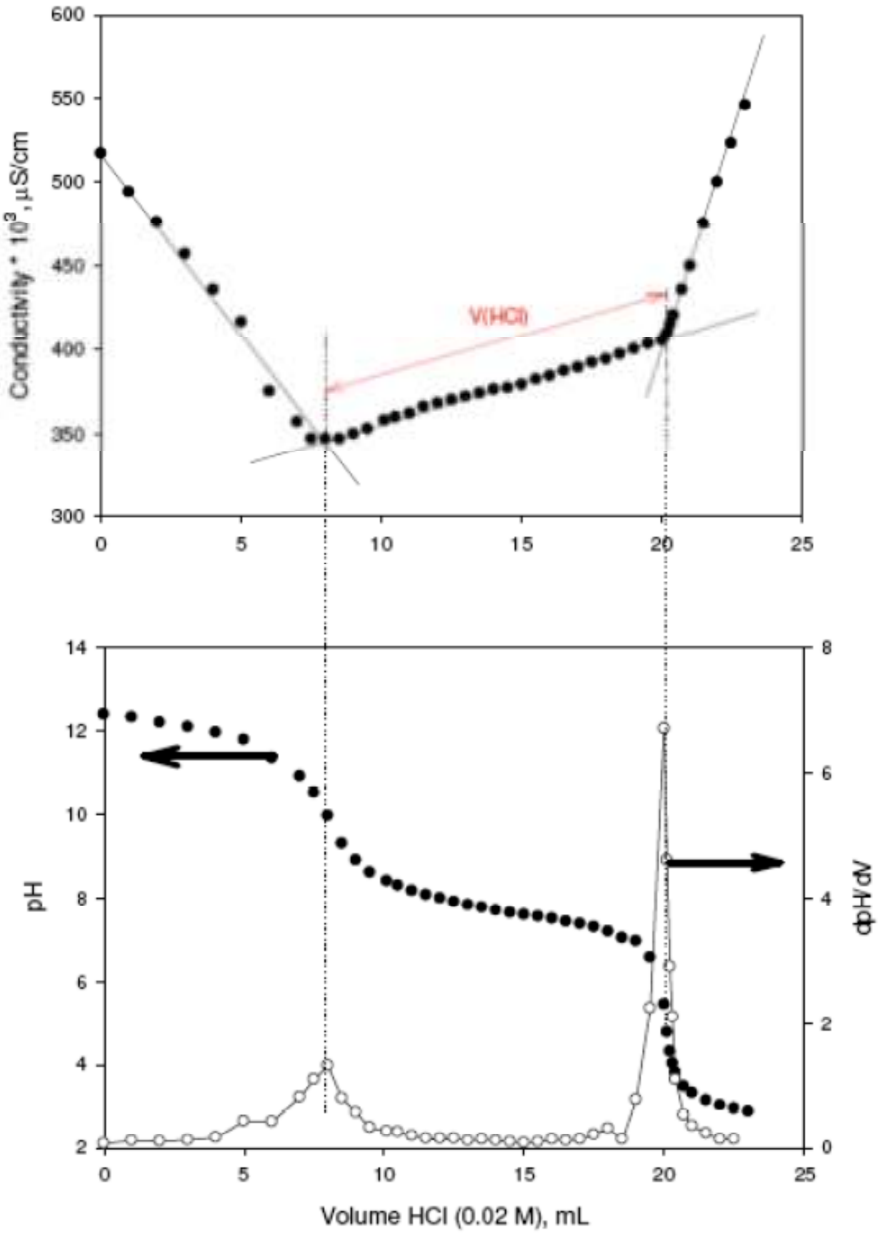

Figure 2.7-S9. Changes in conductivity (**A**) and pH (**B**) as a function of added volume of HCl (0.02 M) for a solution of polymer with 17 mol% of acrylic acid, in THF/aqueous solution containing 0.02 M NaOH illustrating the determination of the carboxylic acid content in the polymer sample.

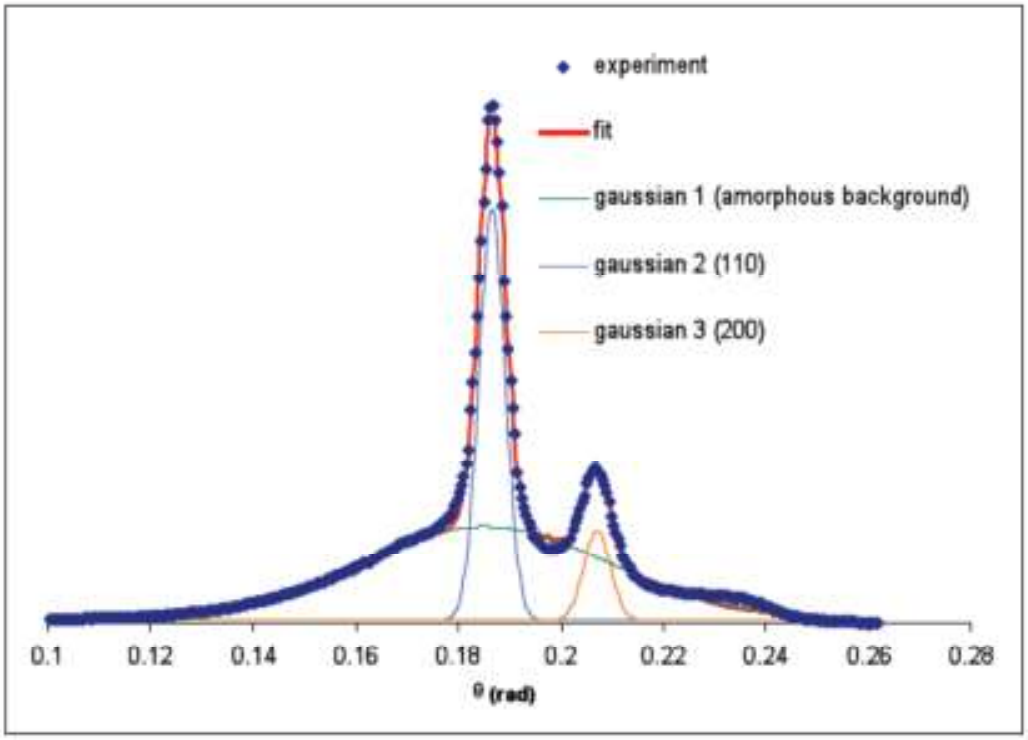

Figure 2.7-S10. Powder X-Ray diffractogram of poly(ethylene-co-AA) containing 7 mol% AA.

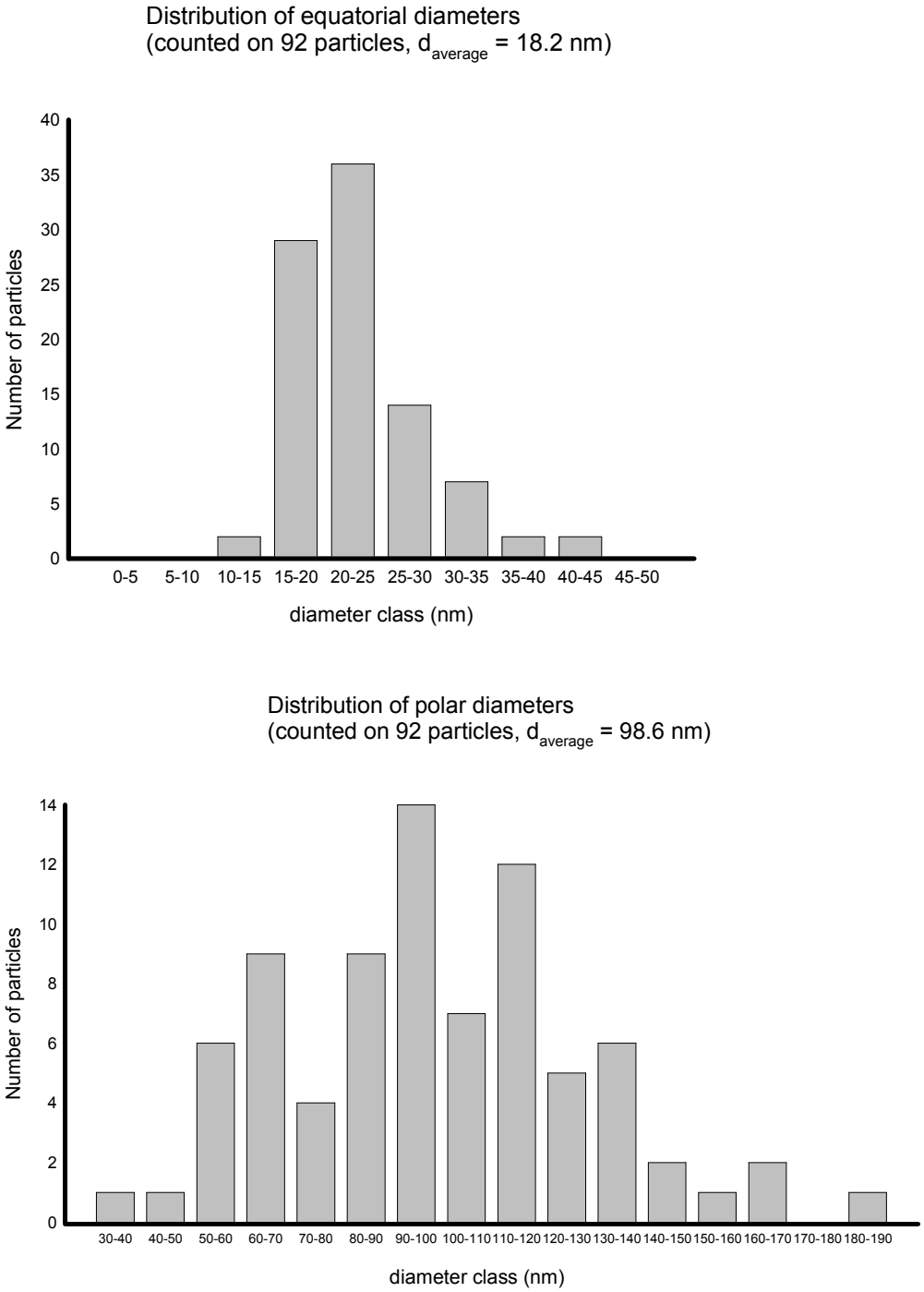

Figure 2.7-S11. Distribution of diameters for PEAA (x = 12%) nanoparticles analyzed by TEM (top: equatorial diameter, bottom: polar diameter).

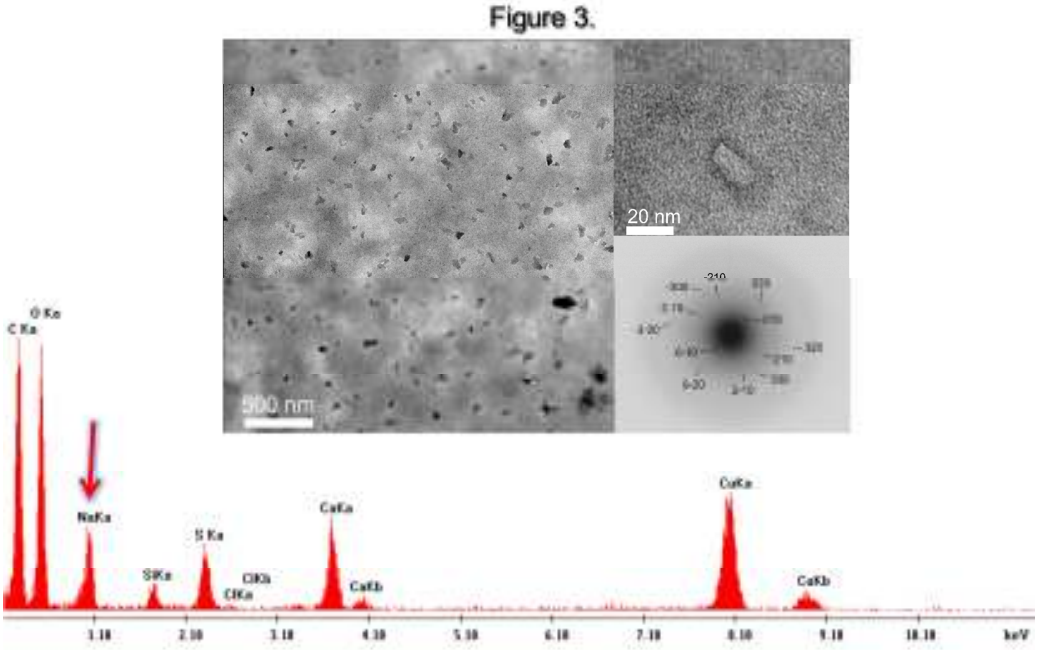

Figure 2.7-S12 Representative Energy dispersive X-Ray spectrum of one of the nanoparticles of *Figure 2.3* (TEM above). The presence of Na is indicative of surface COONa groups. Cu, S, Si and Ca elements are present in virgin grids and are due to the carbon-formvar coating on the Cu grid.

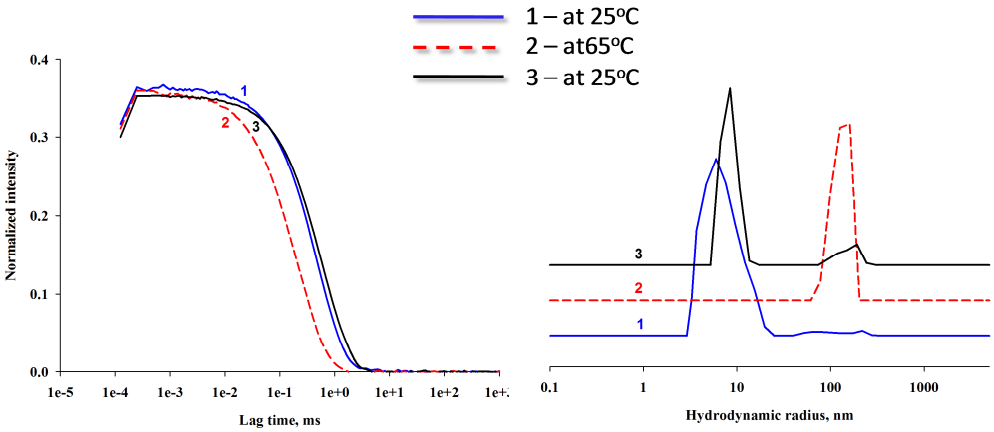

Figure 2.7-S13. Correlation functions and hydrodynamic radius distributions of polymer (PEAA12) colloidal solution presented for three different temperatures: before heating (1; blue line), at maximum temperature (2; red short dashes) and after cooling down (3; black) versus temperature. The data presented here is from a separate experiment than the data shown in *Figure 2.5* from the manuscript body.

2.7.2 References

1. Pan, D.; Williams, T. A.; Senpan, A.; Allen, J. S.; Scott, M. J.; Gaffney, P. J.; Wickline, S. A.; Lanza, G. M. *J. Am. Chem. Soc.* **2009**, *131*, 15522-15527.

2. Chu, L.Y.; Kim, J. W.; Shah, R.K.; Weitz, D. A. *Adv. Funct. Mater.* **2007**, *17*, 2291-2297.

3. Savic, R.; Luo, L.; Eisenberg, A.; Maysinger, D. *Science,* **2003**, *300*, 615-618.

4. Dhar, S.; Gu, F. X.; Langer, R.; Farokhzad, O. C.; Lippard, S. J. *PNAS,* **2008**, *105*, 17356-17361.

5. Kim, K.; Lee, M.; Park, H.; Kim, J.-H.; Kim, S.; Chung, H.; Choi, K.; Kim, I.S.; Seong, B. L.; Kwon, I.C. *J. Am. Chem. Soc.* **2006**, *128*, 3490-3491.

6. Zhou, M.; Xing, F.; Ren, M.; Feng, Y.; Zhao, Y.; Qiu, H.; Wang, X.; Gao, C.; Sun, F.; He, Y.; Ma, Z.; Wen, P.; Gao, J. *Chem. Phys. Chem.* **2009**, *10*, 523-526.

7. Akbulut, M.; Ginart, P.; Gindy, M. E.; Theriault, C.; Chin, K.H.; Soboyejo, W.; Prud'homme, R.K. *Adv. Funct. Mater.* **2009**, *19*, 718-725.

8. Satish, N.; Lyon, L. A. *Angew. Chem.* **2005**, *44*, 7686-7708.

9. Kawaguchi, H.; Fujimoto, K. *Bioseparation,* **1998**, *7*, 253-258.

10. Bergbreiter, D. E.; Case, B. L.; Liu, Y. S.; Waraway, J. W. *Macromolecules,* **1998**, *31*, 6053-6062.

11. Bergbreiter, D. E.; Tian, J.; Hongfa, C. *Chem. Rev.* **2009**, *109*, 530-582.

12. Debord, J. D.; Eustis, S.; Debord, S. B.; Lofye, M. T.; Lyon, L. A. *Adv. Mater.* **2002**, *14*, 658-662.

13. Tant, M. R.; Wilkes, G. L. *Ionomers: synthesis, structure, properties and applications*; Tant, M. R., Wilkes, G. L., Eds.; Chapman & Hall: London, **1997**, p. 261-289.

14. Eisenberg, A. *Macromolecules,* **1970**, *3*, 147-154.

15. Kutsumizu, S.; Schlick, S. *J. Mol. Struc.* **2005**, *739*, 191-198.

16. Szajdzinska-Pietek, E.; Wolszczak, M.; Plonka, A.; Schlick, S. *J. Am. Chem. Soc.* **1998**, *120*, 4215-4221.

17. Baughman, T. W.; Chan, C. D.; Winey, K. I.; Wagener, K. B. *Macromolecules,* **2007**, *40*, 6564-6571.

18. Opper, K. L.; Wagener, K. B. *Macromol. Rapid. Comm.* **2009**, *30*, 915-919.

19. Opper, K. L.; Fassbender, B.; Brunklaus, G.; Spiess, H.W.; Wagener, K. B. *Macromolecules,* **2009**, *42*, 4407-4409.

20. Berda, E. B.; Lande, R. E.; Wagener, K. B. *Macromolecules,* **2007**, *40*, 8547-8552.

21. Breitenkamp, K.; Simeone; J.; Jin, E.; Emrick, T. *Macromolecules,* **2002**, *35*, 9249–9252.

22. Breitenkamp, R. B.; Ou, Z.; Breitenkamp, K.; Muthukumar, M.; Emrick, T. *Macromolecules,* **2007**, *40*, 7617-7624.

23. Kratz, K.; Breitenkamp, K.; Hule, R.; Pochan, D.; Emrick, T. *Macromolecules,* **2009**, *42*, 3227-3229.

24. Tong, Q.; Krumova, M.; Gottker-Schnetmann, I.; Mecking, S. *Langmuir,* **2008**, *24*, 2341-2347.

25. Weber, C. H. M.; Chiche, A.; Krausch, G.; Rosenfeldt, S.; Ballauff, M.; Harnau, L.; Göttker-Schnetmann, I.; Tong, Q.; Mecking, S. *Nano Letters,* **2007**, *7*, 2024-2029.

26. Li, T.; Wang, W. J.; Liu, R.; Liang, W. H.; Zhao, G. F.; Li, Z. Y.; Wu, Q.; Zhu, F. M. *Macromolecules,* **2009**, *42*, 3804-3810.

27. Nakamura, A.; Ito, S.; Nozaki, K. *Chem. Rev.* **2009**, *109*, 5215-5244.

28. Drent, E.; van Dijk, R.; van Ginkel, R.; van Oort, B.; Pugh, R. I. *Chem. Comm.* **2002**, 744-745.

29. Skupov, K. M.; Marella, P. R.; Simard, M.; Yap, G. P. A.; Allen, N.; Conner, D.; Goodall, B. L.; Claverie, J. P. *Macromol. Rapid Comm.* **2007**, *28*, 2033-2038.

30. Skupov, K. M.; Hobbs, J.; Marella, P. R.; Golisz, S.; Goodall, B. L.; Claverie, J. P. *Macromolecules,* **2009**, *42*, 6953–6963.

31. Kochi, T.; Noda, S.; Yoshimura, K.; Nozaki, K. *J. Am. Chem. Soc.* **2007**, *129*, 8948-8949.

32. Skupov, K. M.; Piche, L.; Claverie, J. P. *Macromolecules,* **2008**, *41*, 2309-2310.

33. Luo, S.; Vela, J.; Lief, G. R.; Jordan, R. F. *J. Am. Chem. Soc.* **2007**, *129,* 8946-8947.

34. Piche, L.; Daigle, J.-C.; Poli, R.; Claverie, J. P. *Eur. J. Inorg. Chem.* **2010**, DOI: 10.1002/ejic.201000533.

35. Guironnet, D.; Roesle, P.; Ruenzi, T.; Gottker-Schnetmann, I.; Mecking, S. *J. Am. Chem. Soc.* **2009**, *131*, 422-423.

36. Ma, Q.; Wooley, K. L. *J. Pol. Sci. A: Polym. Chem.* **2000**, *38*, 4805-4820.

37. Otocka, E. P.; Kwei, T. K. *Macromolecules,* **1968**, *1*, 244-249.

38. Jung, M. E.; Lyster, M. A. *J. Am. Chem. Soc.* **1977**, *99*, 968-969.

39. Olah, G. A.; Liang, G.; Schleyer, P. v. R.; Parker, W.; Watt, C. I. F. *J. Am. Chem. Soc.* **1977**, *99*, 968-969.

40. Xiang, M.; Jiang, M.; Kong, X.; Yang, Y.; Lu, W. *Macromol. Rapid Comm.* **1997**, *18*, 385-391.

41. Bandrup, J.; Immergut, E. H., Eds. *Polymer Handbook*; 3rd ed.; Wiley Interscience: New York, **1989**.

42. Takahashi, Y.; Ishida, T. *J. Polym. Sci. Pol. Phys.* **1988**, *26*, 2267-2277.

43. Lehman, S. E.; Wagener, K. B.; Baugh; L.S.; Rucker, S. P.; Schulz, D. N.; Varma-Nair, M.; Berluche, E. *Macromolecules,* **2007**, *40*, 2643-2656.

44. Pecora, R. *J. Nanopart. Res.* **2000**, *2*, 123-131.

45. Tirado, M. M.; Garcia de la Torre, J. *J. Chem. Phys.* **1979**, *71, 2581-2587*.

46. Yin, L.; Chen, J.; Yang, X.; Zhou, E. *Polymer,* **2003**, *44*, 6489-6493.

47. Bauers, F. M.; Thomann, R.; Mecking, S. *J. Am. Chem. Soc.* **2003**, *125*, 8838-8840.

CHAPTER III

General Conclusions

3.1 Conclusions

An initial systematic study was performed to assess the self-assembly of random linear pE-co-AA in aqueous medium. The conditions for successful formation of copolymer nanoparticles in aqueous solution were developed and optimized. This part of work shows the first report on formation of nanoobjects by polyethylene copolymers without the help of surfactants, which are usualy used as colloidal stabilizers. Several characterization methods were applied to study the properties of colloidal nanoparticles solutions, especially their pH and thermoresponsive behaviour. Significant fact is that nanoobjects, formed by the copolymer in aqueous medium, consist of single crystalline polyethylene core and amourphous corona. The latter contains acrylic acid regions, which carboxylic groups provide excellent colloidal stability. Such morphology permits fusion and crystallization of polyethylene core crystal without disrupting the nanoparticle structure. Moreover, it was shown, that thermoresponsive behaviour of the nanoparticles is reversible.

The analysis of bulk copolymer samples showed, that crystallinity and thermal stability depends on the percentage of AA incorporation.

Transmission Electron Microscopy technique was applied to visualize the obtained nanoobjects and Electron Diffraction Technique was used to prove their crystallinity. As a result, copolymer nanoparticles possess non-spherical well-defined shape, with a crystalline core and amorphous corona.

Applications. The studied objects present an interesting family of nanostructured responsive materials with possible applications for biomedical or environmental needs.

3.2 Future Work

It would be interesting to investigate copolymers incorporating AA higher than 12 mol%. Higher fractions of AA will cause stronger microphase separation between AA and oligo-E units, expected to result in the complete disappearance of pE crystallinity. The copolymer nanoparticles will lose their temperature and pH responsive behaviour, but the improved colloidal stability, due to increased hydrophilic AA fraction, may be of interest.